2011

Impact of metallic nanoparticles on photoinduced fluorescence enhancement of colloidal quantum dots

Ali Nejat

IMPACT OF METALLIC NANOPARTICLES ON PHOTOINDUCED FLUORESCENCE ENHANCEMENT OF COLLOIDAL QUANTUM DOTS

by

ALI NEJAT

A THESIS

Submitted in partial fulfillment of the requirements
for the degree of Master of Science
in
The Department of Physics
to
The School of Graduate Studies
of
The University of Alabama in Huntsville

HUNTSVILLE, ALABAMA
2011

In presenting this thesis in partial fulfillment of the requirements for a master's degree from The University of Alabama in Huntsville, I agree that the Library of this University shall make it freely available for inspection. I further agree that permission for extensive copying for scholarly purposes may be granted by my advisor or, in his/her absence, by the Chair of the Department or the Dean of the School of Graduate Studies. It is also understood that due recognition shall be given to me and to The University of Alabama in Huntsville in any scholarly use which may be made of any material in this thesis.

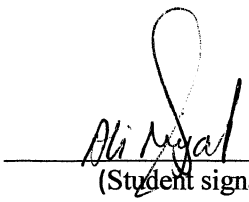

(Student signature) 10-31-2011 (Date)

THESIS APPROVAL FORM

Submitted by Ali Nejat in partial fulfillment of the requirements for the degree of Master of Science in Physics and accepted on behalf of the Faculty of the School of Graduate Studies by the thesis committee.

We, the undersigned members of the Graduate Faculty of The University of Alabama in Huntsville, certify that we have advised and/or supervised the candidate on the work described in this thesis. We further certify that we have reviewed the thesis manuscript and approve it in partial fulfillment of the requirements for the degree of Master of Science in Physics.

Committee Chair

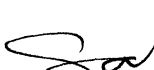
10/31/2011 Dr.Seyed Sadeghi

(Date)


11/1/11 Dr.Lingze Duan


Dr.James K. Baird

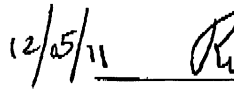
12/5/11 Department Chair


11/1/11 College Dean


12/5/11 Graduate Dean

ABSTRACT

The School of Graduate Studies

The University of Alabama in Huntsville

Degree Master of Science College/Dept. Science/Physics

Name of Candidate: Ali Nejat

Title: Impact of Metallic Nanoparticles on Photoinduced Fluorescence Enhancement of Colloidal Quantum Dots

We studied emission of colloidal semiconductor quantum dots in the presence and absence of metallic nanoparticles as they were irradiated with a laser beam. For this, we first used numerical calculations to find extinction coefficients of different types of metallic nanoparticles. Gold metallic nanoparticles were then fabricated with two techniques: i) thermal evaporation of gold thin film on a substrate followed by thermal annealing, and ii) electron beam lithography. The sizes of the metallic nanoparticles were optimized to achieve significant amount of plasmonic enhancement of quantum dots emission. Our results show photo-induced fluorescence enhancement of CdSe/ZnS quantum dots can be dramatically suppressed in the presence of metallic nanoparticles. Additionally, we demonstrate at a certain intensity of the laser field the emission of the quantum dots rolls over, making the quantum dots quite inefficient emitters. We showed such processes were caused by plasmonic near field enhancement of the metallic nanoparticle and sudden activation of photoionization process.

Abstract Approval: Committee Chair

Department Chair Richard Liou (for Dr Zank) 12/05/11

Graduate Dean Rhonda Kay Gaede 12/5/11

ACKNOWLEDGMENTS

My sincere gratitude and appreciation goes to my advisor, Dr. Seyed Sadeghi, for his patient guidance and supports during my graduate studies at the University of Alabama in Huntsville. Also, I have the pleasure of thanking the advisory committee members, Dr. James k. Baird and Dr. Lingze Duan.

I also wish to thank Dr. Williams and Dr. Linquist for access for me to use NMDC and Dr. Yongbin Lin and Frank Berisford for all their guidance during my research.

I would have not been able to finish this work without the encouragement and support of my parents, Homa and Mehdi.

At the end I would like to thank my friends Siavash Neshatpour, Alireza Chenani, Robert West and Kira Patty for helping me in editing this thesis.

TABLE OF CONTENTS

Page

LIST OF FIGURES

LIST OF TABLES

CHAPTER 1

1INTRODUCTION

Fluorescence semiconductor nanocrystals due to their exceptional properties such as broad emission wavelength range and nano-scale dimension etc., are very promising candidates for developing new sensors, optical devices, etc. [1-2]. In this chapter, I review surface Plasmon and localized Plasmon resonance and discuss their applications as sensing materials. In Chapter 2, I will explain two fabrication techniques of metallic samples that can support localized surface plasmons.

In addition, in this chapter, I will study Quantum Dot (QD) solids and review the mechanisms behind photo-induced fluorescence enhancement (PFE). The PFE of QDs solids have been widely investigated by other groups [22]. The impact of localized surface plasmons on a PFE process, however, has not been studied so far. In Chapter 4, I investigate the dynamic emission of QDs in vicinity of metallic nano particles as function of laser intensity and time and impact of metallic nanoparticles on PFE.

1.1 Introduction to Surface Plasmons Resonance (SPR)

Due to the diffraction limit, even with an optical system, we cannot focus light to a nanoscale spot size. But with surface plasmons, also known as Surface Plasmon polaritons Resonance (SPR), which are electromagnetic (EM) waves that propagate along the surface of a conductor, we are able to do that [3]. Since the EM wave is on the boundary of the metal and the external medium (such as air). This interaction causes the free electrons in the metals to oscillate on a collective frequency. These oscillations are

very sensitive to any changes on the boundary, such as the adsorption of molecules to the metal surface [4]. When excited, surface plasmons propagate in a wave-like fashion along the planar interface and the amplitude decays exponentially with the distance into each medium from the interface. In this chapter we start with Maxwell's equation to study SPRs.

1.2 Maxwell's Equation

In this section the electromagnetic theory that describes the main characteristics of Surface Plasmons (SPs) will be explained. We begin with an introduction to Maxwell's equations and also the wave equations to find the refractive index which at the end will lead us to calculate the dispersion relation for bulk metals (in the free electron gas model) which will enable us to describe the optical properties of metals.

The differential forms of Maxwell's equations are [5]

$$\nabla . \vec{D} = \rho \tag{1.1}$$

$$\nabla . \vec{B} = 0 \tag{1.2}$$

$$\vec{\nabla} \times \vec{E} = -\frac{\partial \vec{B}}{\partial t} \tag{1.3}$$

$$\vec{\nabla} \times \vec{H} = \frac{\partial \vec{D}}{\partial t} + J \quad . \tag{1.4}$$

The electromagnetic fields in empty space are given in terms of two vectors, $\vec{E}$ and $\vec{B}$, called the electric field vector and magnetic field respectively. In the presence of matter we will have $\vec{D}$ as an electric displacement and $\vec{H}$ as magnetic field vector. ρ is the charge density and J is the current density.

In the presence of matter we can use the constitutive relation which is [5]

$$\vec{D} = \varepsilon_0 \vec{E} + \vec{P}(\vec{E}) = \varepsilon \vec{E} \quad . \tag{1.5}$$

When we apply a field to the material, it gets polarized due to the displacement of charges. The external field causes a redistribution of charges and hence induces the polarization. In equation 1.5, $\vec{D}$ is the displacement vector which is the sum of the electrical field and the polarization vector, $\vec{P}(\vec{E})$, and ε_0 is the dielectric constant of vacuum, which is $8.85 \times 10^{-12}\ C^2 N^{-1} m^{-2}$ and ε is the material dependent dielectric permittivity constant.

The magnetic field can introduce in the same way [5]:

$$\vec{B} = \mu_0 \vec{H} + \mu_0 \vec{M}(\vec{H}) \quad , \tag{1.6}$$

where μ_0 is the permeability of free space and $\vec{M}(\vec{H})$ is the magnetic polarization vector. In our case, we do not have any magnetization. Therefore, we set $\vec{M}(\vec{H})$ to be zero.

1.3 Dispersion Relation for Light

To analyze wave propagation in a charge free medium, we need to introduce a wave equation for $\vec{E}$ [5]:

$$\nabla^2 \vec{E}(r,t) = \frac{\varepsilon_r}{C^2} \frac{\partial^2 \vec{E}(r,t)}{\partial^2 t^2} \quad , \tag{1.7}$$

where [5]

$$\vec{E}(r,t) = Re\{\vec{E}(r,\omega) \exp\left(i\vec{k}.\vec{r} - i\omega t\right)\} \tag{1.8}$$

$$n = \frac{c}{v} = \sqrt{\varepsilon_r} = \sqrt{1 + \chi} \tag{1.9}$$

$$\vec{P} = \varepsilon_0 \chi \vec{E} \quad . \tag{1.10}$$

In equation 1.9, n is the refractive index, ε_r is the relative dielectric constant or the relative permittivity and χ is the electric susceptibility which is constant for materials which are homogenous and isotropic [5].

Substituting E, in the wave equation, we can calculate the dispersion relation to be [5]

$$\omega = \pm \frac{c}{n} k \quad . \tag{1.11}$$

For a wave propagating in a vacuum, the refractive index is n=1 and the dependence of ω on k is shown in Figure 1.1 by the red line, which should be referred to as a light line. On the other hand, for a wave propagating in a medium such as metal, for plotting the dispersion relation we need to first find the refractive index, since it is no longer constant, as depends on the frequency of the incident light.

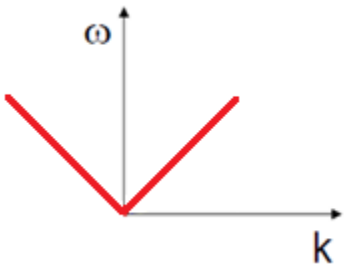

Figure 1.1 Disperstion relation graph for light line [6].

1.4 Dispersion Relation for Bulk Metals

To find the metal's refractive index (in the free electron gas model), consider the time varying field (E) and use Newton's second law, [7]. Then,

$$E(t) = Re\{E(\omega)\exp(-i\omega t) \tag{1.12}$$

$$\vec{F} = m\vec{a} \tag{1.13}$$

$$m\frac{dr^2}{dt^2} = e\vec{E} \tag{1.14}$$

$$P(t) = -er(t) \quad , \tag{1.15}$$

where $P(t)$ is the dipole moment of the electron and the harmonic time dependence of P is given by:

$$P(t) = Re\{P(\omega)\exp(-i\omega t)\} \quad . \tag{1.16}$$

Substituting equation 1.16 in equation 1.15, then equation 1.14 can be rewritten as

$$-m\omega^2 P(\omega) = e^2 E(\omega) \quad . \tag{1.17}$$

Rearranging the above equation give

$$P(\omega) = -\frac{e^2}{m}\frac{1}{\omega^2}E(\omega) \quad . \tag{1.18}$$

Now we can rewrite equation 1.9 with substituting equation 1.18 in equation 1.10 to get the dielectric constant relation [7]

$$\varepsilon_r = 1 + \chi = 1 + \frac{NP(\omega)}{\varepsilon_0 E(\omega)} = 1 - \frac{Ne^2}{\varepsilon_0 m}\frac{1}{\omega^2} = 1 - \frac{{\omega^2}_p}{\omega^2} \quad , \tag{1.19}$$

where N is the number of electrons and ω_p is the plasma frequency, which is an intrinsic property of materials [7]

$$\omega_p{}^2 = \frac{Ne^2}{\varepsilon_0 m} \quad . \tag{1.20}$$

We can now see from the relative dielectric relation (equation 1.19), the frequency dependency. Also it can be seen that when the light frequency is less than the plasma frequency, the relative dielectric becomes negative, which means light cannot penetrate through the metal since n is the square roots ofε_r, and hence n will become purely imaginary and wave won't propagate and it will exponentially decay through the metal and this is why metals act like mirrors.

We can rewrite equation 1.11 to be

$$\omega^2 \varepsilon_r = c^2 k^2 \quad . \tag{1.21}$$

Then substitute equation 1.19 in equation 1.21 to get the dispersion relation for bulk materials to be

$$\omega = \sqrt{\omega_p{}^2 - c^2 k^2} \quad . \tag{1.22}$$

A plot for the dispersion relation based on equation 1.22 for bulk materials has been shown in Figure 1.2. clearly, the dispersion relation is not linear, the curve red line lies above the light line. In general $\hbar\omega_p$ is around 10ev for bulk metals.

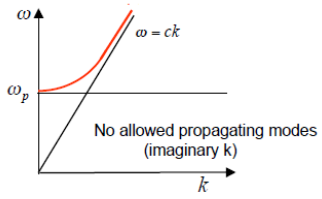

Figure 1.2 Dispersion relation graph for bulk metal [6].

1.5 Dispersion Relation for Surface Plasmon Polaritons Resonance (SPR)

As mentioned before SPRs are electromagnetic waves that propagate on the surface of metal and dielectric interface. These electromagnetic waves cause oscillation of the free electrons in the metal-dielectric interface. To study SPRs we need to utilize Maxwell's equation of electromagnetic waves at interface of metal and conductor[8]. In Figure 2.3, we can see how field distribution and charge distribution in boundary of metal-dielectric interface.

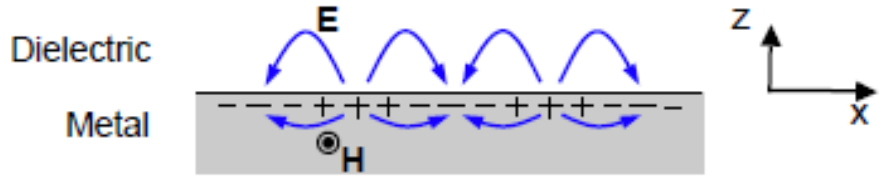

Figure 1.3 SPR modes which propagate in x direction in presence of electric field [6].

Using the Maxwell's equations (1.1-1.4), for the electric and magnetic vectors for above situation in boundary metal-dielectric interface, we will have the following :

For z > 0

$$H_d = \left(0, H_{yd}, 0\right)\exp\left[i(k_{xd} + k_{zd}z - \omega t)\right] \tag{1.23}$$

$$E_d = (E_{xd}, 0, E_{zd})\exp\left[i(k_{xd} + k_{zd}z - \omega t)\right] \tag{1.24}$$

For z < 0

$$H_m = \left(0, H_{ym}, 0\right)\exp\left[i(k_{xm}x + k_{zm}z - \omega t)\right] \tag{1.25}$$

$$E_m = (E_{xm}, 0, E_{zm})\exp\left[i(k_{xm}x + k_{zm}z - \omega t)\right] \quad , \tag{1.26}$$

where ω is the frequency of the light incident on the metal and dielectric interface.

Having in mind that the electric and magnetic field should be continuous at the border we can write these boundary conditions:

$$E_{xm} = E_{xd} \qquad \varepsilon_m E_{zm} = \varepsilon_d E_{zm} \qquad H_{ym} = H_{yd} \quad . \tag{1.27}$$

As long as we do not have any charges and currents in the surface (J=0) we can rewrite equation 1.4 to be

$$\nabla \times H_i = \varepsilon_i \frac{\partial E_i}{\partial t} \quad . \tag{1.28}$$

By replacing *H* and *E* from equations 1.23 to 1.26 in equation 1.28 and applying the boundary conditions 1.27 for magnetic and electric field which say that they should be continuous on the interface of the dielectric and metal medium, we can by some simple algebra find the relation between the wave vector, k, and relative permittivity, ε_r :

$$\frac{k_{zm}}{\varepsilon_m} = \frac{k_{zd}}{\varepsilon_d} \quad . \tag{1.29}$$

For any electromagnetic wave:

$$k_x^2 + k_{zi}^2 = \varepsilon_i \left(\frac{\omega}{c}\right)^2 \quad . \tag{1.30}$$

And with using equation 1.29 and substituting it in equation 1.30 we can find k_x which is [6]

$$k_x = \frac{\omega}{c}\left(\frac{\varepsilon_m \varepsilon_d}{\varepsilon_m + \varepsilon_d}\right)^{\frac{1}{2}} \quad . \tag{1.31}$$

Recalling the relation for relative permittivity of metals versus frequency, and assuming the relative permittivity for the dielectric to be constant, it can plotted as

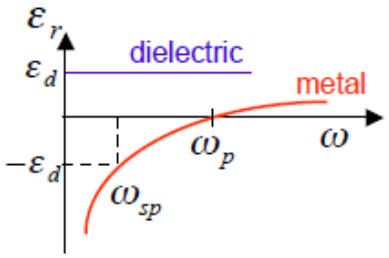

Figure 1.4 Relative permittivity of dielectric and metal graph as a function of frequency [6].

in Figure 1.4. It can be seen that the permittivity of the dielectric is not dependent on the wavelength or frequency of the incident light, which just means dielectric materials have the same permittivity throughout all frequency ranges. For metals the permittivity is strongly dependent on the frequency and as it can be seen from the dispersion relationship we have a resonance at $\varepsilon_m = -\varepsilon_d$ [5]. Notice that based on equation 1.31, k goes to infinity when $\varepsilon_m = -\varepsilon_d$ at the denominator.

For plotting the dispersion relation for SPRs, we need to use the relation between relative permittivity of metal and frequency (Figure 1.4), where for metals, in the low frequency limit, ε_m goes to minus infinity, having this in mind and taking the limit of equation 1.31, we can plot the dispersion relation for surface Plasmon (Figure 1.5)

$$k_x = \frac{\omega}{c}\lim_{\varepsilon_m \to -\infty}\left(\frac{\varepsilon_m \varepsilon_d}{\varepsilon_m + \varepsilon_d}\right)^{\frac{1}{2}} \approx \frac{\omega}{c}\sqrt{\varepsilon_d} \quad . \tag{1.32}$$

The Surface Plasmon frequency is defined when $\varepsilon_m = -\varepsilon_d$. With this condition the wave vectors go to infinity. The surface plasmon frequency will be denoted by $\omega = \omega_{sp}$.

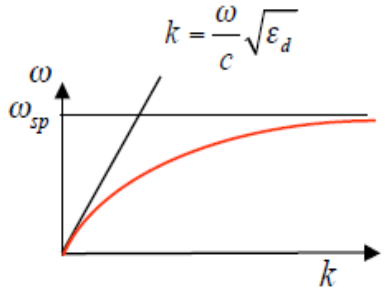

Figure 1.5 Dispersion relation graph for SPRs at interface of metal and dielcetric [6].

We can see in the dispersion relation for surface plasmon graph (Figure 1.5) that the surface Plasmon for metals and dielectrics interface, lie below the light line which means there is no coupling between the light line and the SPR modes. It means if we use laser beam as excitation source for SPRs, we need to use some trick to excite SPRs modes on the interface metal-dielectric.

1.6 Excitation of the SPRs with Light

It is very interesting to couple a light with a few hundred nanometers wavelength, a structure the size of a few nanometers. Recall from in Figure 1.5 there is no intersection between the SPRs(red line) and the light line; in other words, if a far field laser is radiated on a system which supports SPP modes, it cannot get coupled, so we need to find some trick to get the SPP modes excited.

One trick is to excite the SPP modes from a higher index medium to a lower one [9]. It can be seen in Figure 1.6 that when the SPP modes are excited from a higher index medium, then the light line slope is lowered and there will be an intersection between the SPP modes and the light line. To introduce higher index medium require as specific setup which is called the Kretschmen geometry [9].

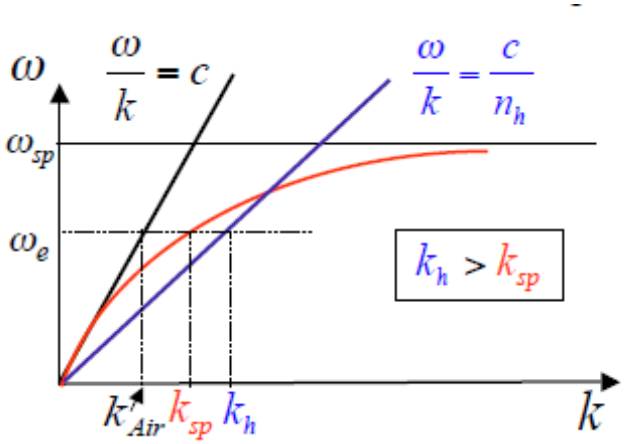

Figure 1.6 Excitation SPP at metal/air interface from high index medium $n=\boldsymbol{n_h}$ [6-12].

In this geometry we have a prism (typically made of silicon dioxide) coated with a thin metal film. The metal film is thin enough to allow evanescent modes. The incident light beam impinges on one face of the prism towards the metal-dielectric interface

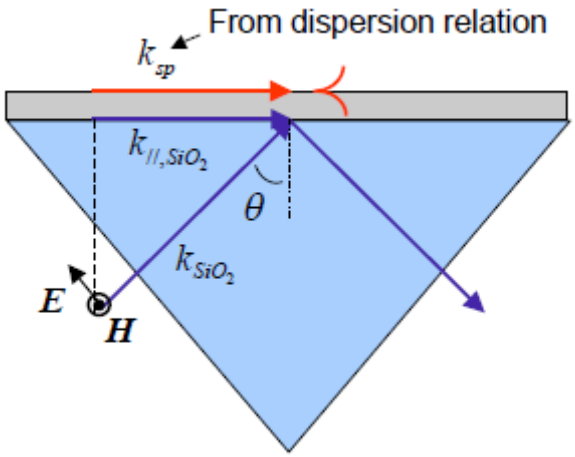

Figure 1.7 Kretschmann Geometry [6-12].

(Shown in Figure 1.7). we will use the total internal reflection of the metal-dielectric interface. With this setup, evanescent modes are produced at the far end of the dielectric which is closer to the air. Since evanescent modes are away from the metal-dielectric interface, SPR modes are not generated at the metal-dielectric interface. In fact the purpose of this geometry is to match the energy and momentum of incident light to SPR,

to produce a strong coupling between the incident light and the surface Plasmon mode at the metal-air interface [12]. This effect is shown in Figure 1.8.

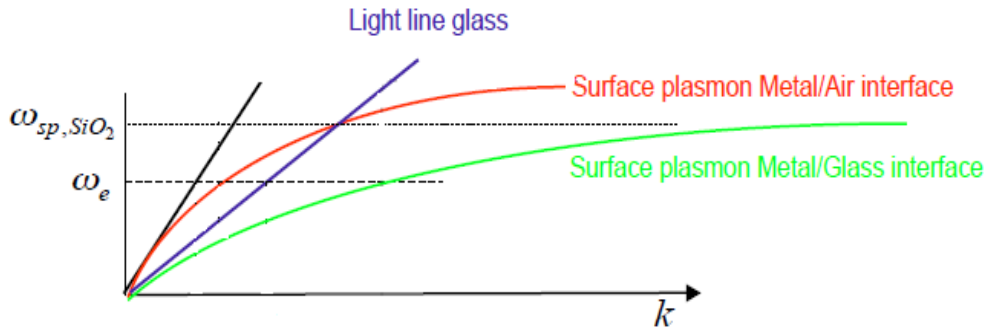

Figure 1.8 Dispersion graph shows Kretschmann setup enables excitation surface plasmon at air/metal interface [6-12].

This setup is very useful since the SPP modes are outside of our system and be used for any application desired. To have some qualitative description of the coupling of the light beam to the SPP modes, we are looking for the case when there is no reflection, and thus there would be a maximum coupling of the SPP modes. Obviously the no reflection case is an ideal case, and in actuality there will always be some imperfections. Instead we will look for the case when the reflection is at its minimum which corresponds to the case when the reflection curve in Figure 1.9 is at its lowest.

As an example of how this setup can be used for biological sensors based on the Kretschmen geometry, where a focused polarized light is radiated on the prism towards the metal-dielectric interface, they use a gold film as the metal and then they look at the reflected light in the same way that we showed before, except that, this time they have a flow channel on the far side of the gold layer and attached to it a little receptor (shown in red in Figure 1.10).

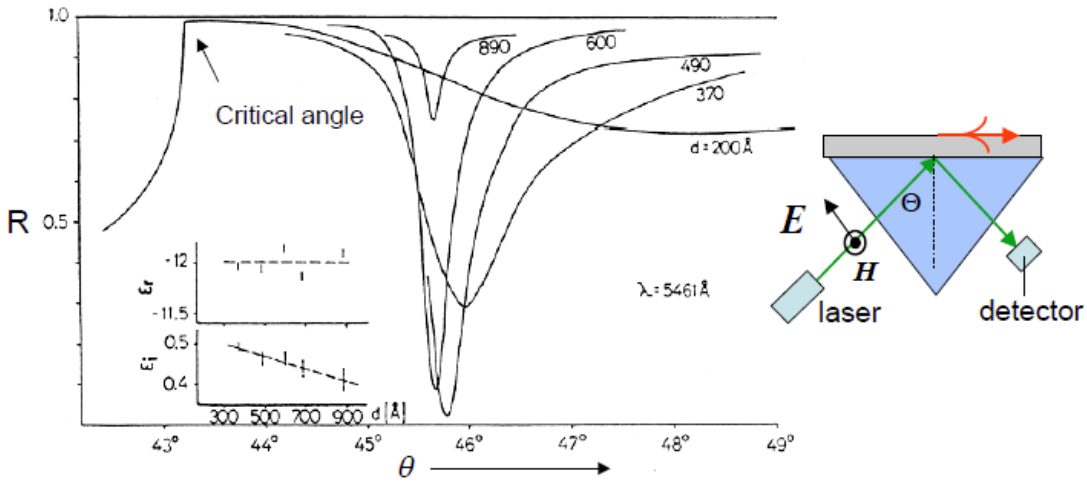

Figure 1.9 As you can see this technique can be used to determine the thickness of metallic thins film [6-10].

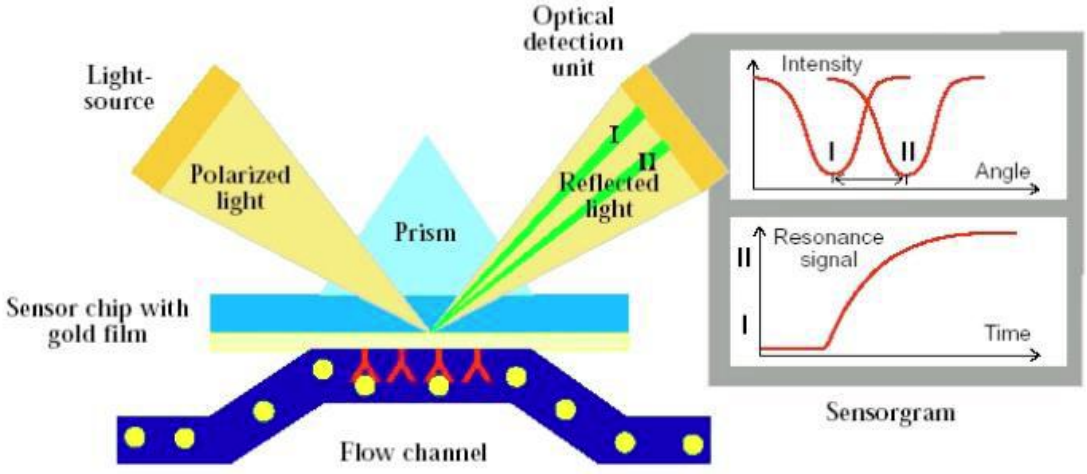

Figure 1.9 Sensor schematic shape [11-6].

When the biological materials attached to the receptor cause some changes for the incoming light due to their change in the relative permittivity of the environment, it

will result in a shift in the reflection angle which caused the maximum coupling of light to the metal for making SPP modes [9].

Another way to excite the SPP modes is using grating structures [29], in this way under certain conditions where the grating is produced properly, the momentum of the incident light can directly get matched to the surface Plasmons along the grating.

1.7 Localized Surface Plasmon Resonance (LSPR)

Localized Surface Plasmons Resonance (LSPR) are charge density oscillations, confined to metallic nanoparticle [8]. Excitation of localized surface Plasmons by an electric field at an incident wavelength where the resonance occurs, results in a strong light scattering and an enhancement of the local electromagnetic fields.

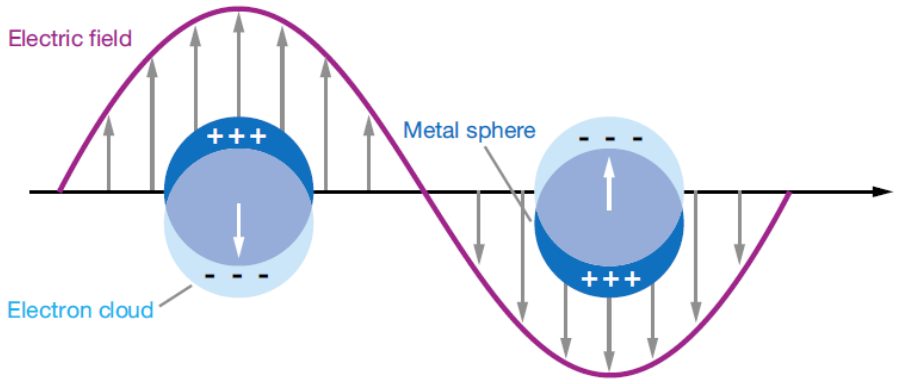

Figure 1.10 A localized surface plasmon [8].

This can only happen in the presence of intense surface Plasmon absorption bands. The frequency and intensity of the surface plasmon absorption bands are a characteristic of the material (typically gold, silver, etc.) and are highly sensitive to the

size and shape of the metallic nanoparticles, as well as to the environment which surrounds them [8].

Additionally, LSPs have applications in manipulating fluorescence nanocrystal emissions and as nanophotonics devices, switches, information storage, and as sensors [8].

1.8 Excitation of LSRP

The excitation of the localized surface plasmons, in contrast to surface plasmon polaritons, is very easy to achieve and more practical, since for the excitation we don't need any special geometry as long as we have metallic nanoparticles (MNP) and radiate them with a light beam (laser) which has a wavelength less than the Plasmon frequency of our metallic nanoparticles [8].

Localized Surface Plasmon (LSP) are very useful for sensing applications and fluorescence dyes since the electric field of the metallic nanoparticles gets enhanced in a certain band of frequency, and that can increase the radiative decay rate, leading to photoluminescence enhancement of the dye [34].

Maxwell's equations are used to calculate the electric field outside the metallic nanoparticles. The simplest case is a spherical shape for the metal with radius "*a*" where *a* is much smaller than the incident wavelength λ (a/λ <0.1) [8]. In this special case, to solve Maxwell's equation a quasi-static approximation method is used [8] and the boundary conditions to derive the final equation. The boundary conditions are applied for this case are [8]

$$E_{out}(x, y, z) \rightarrow E_0\hat{z} \quad as\ r \rightarrow \infty \tag{1.33}$$

$$E_{in}(x,y,z) \to finite \quad as\, r \to 0 \tag{1.34}$$

$$\varepsilon_{in} E_{r,in} = \varepsilon_{out} E_{r,out} \quad . \tag{1.35}$$

And also it should be noted that E_θ and E_φ are continuous at the boundary. After applying the boundary conditions, the electric field outside the nano-metallic sphere is [8]

$$E_{out}(x,y,z) = E_0\hat{z} - \left[\frac{\varepsilon_{in}-\varepsilon_{out}}{(\varepsilon_{in}+2\varepsilon_{out})}\right] a^3 E_0 \left[\frac{\hat{z}}{r^3} - \frac{3z}{r^5}(x\hat{x}+y\hat{y}+z\hat{z})\right] \quad , \tag{1.36}$$

where

$$\varepsilon_{in}(\omega) = 1 - \frac{\omega_p^2}{\omega(\omega - i\Gamma(a))} \quad . \tag{1.37}$$

In this equation, ε_{in} [13] is the relative permittivity of the metallic nanoparticle, ε_{out} is the permittivity of the environment which hosts our metallic nanoparticle, and ω is frequency of incident light. $\Gamma(a) = \Gamma_\infty + \frac{Av_f}{a}$ is the electron scattering rate of the MNP, where Γ_∞ is the bulk-like electron scattering rate considered equal to 0.1 eV [13] and $v_f = 1.4 \times 10^8\ cms^{-1}$ is the Fermi velocity. A is a model dependent constant taken to be equal to one. When $\varepsilon_{in} = -2\varepsilon_{out}$, the local electric field is enhanced relative to the incident electric field. (It should be noted that the permittivity of metals (ε_{in}) are strongly dependent on the incident wavelength). Metals such as silver, gold, chromium etc. show this enhancement in local electric field at a visible frequency [14]. Since there are oscillation charges on the surface of the MNP, the size and shape of the Metallic nanoparticle play an important role in the enhancement of the field another factor in this enhancement is the permittivity of the host medium. In Chapter 2, we used Mie Theory

for our numerical calculation for finding the localized surface plasmons for sphere shape of metallic nanoparticles.

1.9 Nanocrystal Quantum Dots (QD's)

The Semiconductor nanocrystals, known as quantum dots (QDs), are one of the prominent nanomaterials. Since it is possible for QDs to have excitation modes which are confined in 3 dimensions, they can demonstrate properties in between bulk material and discrete molecules [15]. QDs can become excited when they are illuminated with photons with energy higher than the band gap. So when carrier relaxation of QDs takes place, QDs can emit photons. An interesting feature is their emission energy is adjustable, since due to quantum confinement effects for which a change in the composition or/and size of the QDs can lead to a change in the energy of the emitted photon [16]. Due to their photoluminescence properties, QDs are the prime subject for sensors [18], Solar Cells, optical devices [17], semiconductor lasers [15], etc. QDs also have been used for labeling of biological targets which is useful for diagnosing diseases such as cancer [1-2].

QDs are semiconductor nanocrystals with a nano scale size of a few nanometers from 1nm to 60nm. Due to the small size of the nanocrystals, we have spatial 3D confinement. This 3D confinement distinguishes QDs from bulk semiconductors, which have continuous conduction and valance energy bands. Due to the quantum confinement (3D confinement), the QD's have discrete bands of energy in valance and conduction bands [15].

1.10 Quantum Confinement

For determining the electronics structure of QDs it is necessary to find what happens to a bulk semiconductor when it is shrinking to nano scale. For this analysis the density of states (DOS) must be determined, and indicting the impacts of the 3D restrictions on the carriers' motion. "The DOS is the number of states per interval of energy at each energy level that are available to be occupied"[19]. From the dispersion relation of bulk semiconductors, we can derive the DOS for different degrees of freedom can be derived, in Table 1.1 [19]. For different degrees of freedom, the density of state is different and due to quantum confinement for a zero degree of freedom, DOS becomes discrete.

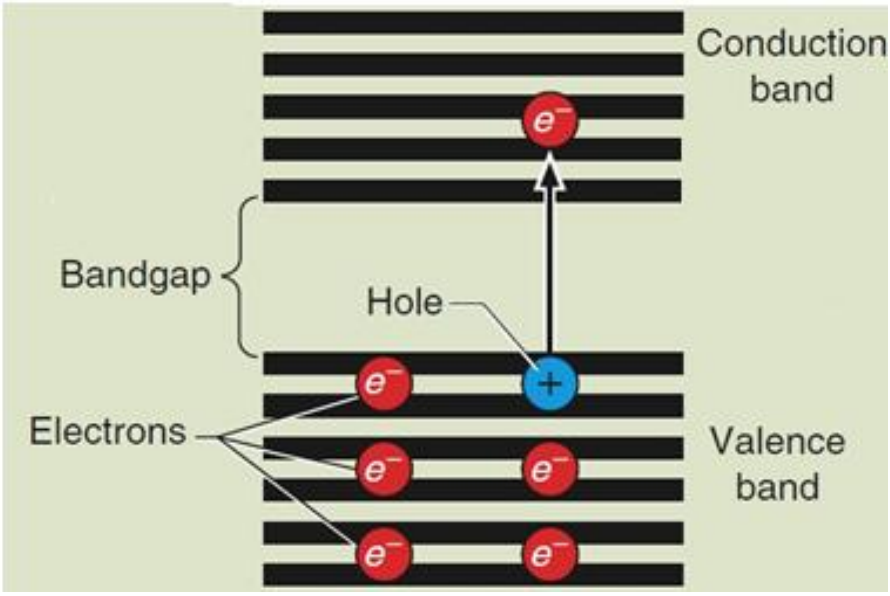

Figure 1.11 The conduction and valance bands of the semiconductor when excited by irradiated light show exciton where exciton is generated by electron and hole pair by incident light.

Quantum confinement plays a significant role when the size of semiconductor nanocrystals is smaller than the Bohr excitation radius. The Bohr excitation radius is the distance between the electron and the hole, when a light interacts with a semiconductor nanocrystals and create exciton (electron hole pairs).

Table 1.1 DOF for Bulk and Quantum well and Quantum Wire and Quantum Dots semiconductors [19].

Degrees of freedom	Density of state	Graph
3(Bulk)	$\rho = \frac{1}{2\pi}\left(\frac{2m^*}{\hbar^2}\right)^{\frac{3}{2}}\sqrt{(E-E_C}$	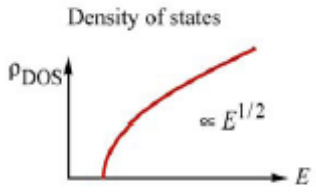
2(Quantum Well)	$\rho = \frac{m^*}{\pi\hbar^2}\sigma(E-E_C)$	
1(Quantum wire)	$\rho = \frac{m^*}{\pi\hbar}\sqrt{\frac{m^*}{2(E-E_C)}}$	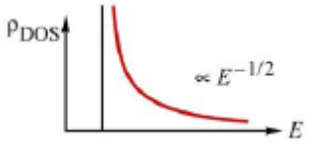
0(Quantum Dot)	$\rho = 2\delta(E-E_C)$	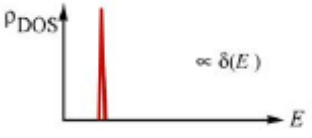

If the light beam has enough photon energy, it can produce an electron-hole pair where an electron will be created in the conduction band and there will be a hole in the valance band. The distance between this hole in the valence band and the electron in the conduction band is called the Bohr exciton radius [15].

To calculate exciton Bohr exciton radius, we can use the Hydrogen Bohr radius, a_0, from (equation 1.38) and substitute it in Bohr exciton radius ($a_{exciton}$) equation 1.39 to calculate the Bohr exciton radius, $a_{exciton}$, for different materials in equation 1.39

$$a_0 = \frac{4\pi\varepsilon_0\hbar^2}{m_e e^2} = 0.529\text{Å} \tag{1.38}$$

$$a_{exciton} = \frac{a_0\varepsilon}{m^*/m_e} \tag{1.39}$$

$$m^* = \frac{m_e^*.m_h^*}{m_e^*+m_h^*} \quad , \tag{1.40}$$

where m^* is the reduced effective mass of the electron-hole which can be calculated using equation 1.40 and m_e is the mass of the electron and m_e^* , m_h^* are the effective mass of the electron in the conduction band the and the effective masses of the hole in the valance band respectively. ε is the dielectric permittivity in the bulk material.

In Table 1.2 you can see the Bohr exciton radius for different materials. As mentioned before, for having the quantum confinement effect in nanocrystals relies upon the size of the nanocrystals being less than the Bohr excitation radius.

The energy band gap in semiconductor nanocrystals is more than the band gap of the bulk form of the same material.

Table 1.2 Bohr excitation radius for different types of materials .

Type of materials	Si	Ge	GaP	GaAs	InP	CdSe	InSb
$a_{excitation}\ (nm)$	4.2	17.7	1.7	14	9.5	3	69

The Band gap for nanocrystals can be calculated using equation 1.41 [15] :

$$E_g^{NP} = E_g^{bulk} + \frac{h^2\pi^2}{2m^* d_{NP}^2} \quad . \qquad (1.41)$$

As is seen in equation (1.41) and in Figure 1.13 as the particle size becomes smaller, the band gap energy becomes larger. Therefore a QD's of smaller size emit at shorter wavelength and vice versa.

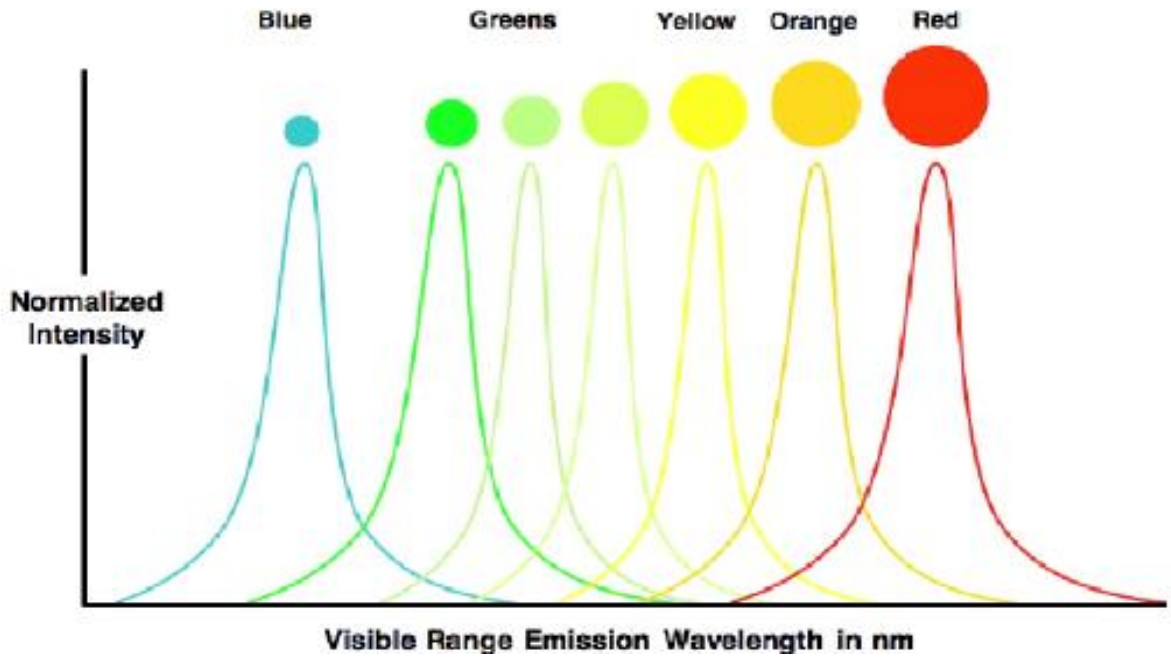

Figure 1.12 Effect of size to the emission of light of QDs.

1.11 Nano Crystal (NC) Fabrication

There are two common types of nanoparticles:

- Epitaxial nanoparticles
- Colloidal nanocrystals

Epitaxial nanoparticles are grown by molecular beam epitaxy on a substrate to which the material is not lattice matched. This can lead to de-wetting and islanding of the material which produce the nanocrystals. For this to happen the substrate should be chosen in such a way that the energy between the film and the substrate is high enough [20].

Colloidal nanocrystals are nanoparticles that are grown by an organo-metallic chemical synthesis (Figure 1.14) or the La mer model [16-20]. These types of nanocrystals are produced by the injection of precursors into a high temperature (250℃) solvent. The precursors should be organo-metallic (such as dimethyl cadmium and trioctylphosphine selenium) while the solvent is a mixture of organic molecules (such as trioctylphosphine oxide or oleic acid) [16-20]. Interactions between the metallic and non-metallic ions result in the formation of the core which can grow to become nanocrystals. To stop the growth of the core/nanocrystals, they are taken out of the solution and cooled down to room temperature. The temperature of the solvent and the amount of time the nanocrystal spend in the solution determines their size and hence their emission wavelength. The colloidal nanocrystals have a very narrow particle size distribution, as well as being soluble in a wide range of organic solvents or water. This solubility is due to the overcoating of the core with a monolayer of organic surface ligands. These

two characteristics are specific to colloidal nanocrystals and epitaxial nanoparticles do not have these properties.

1.12 QD Types and Their Applications

Usually QDs are composed of binary semiconductors consisting of column II-VI elements in the periodic table like Cadmium Sulfide (CdS), Cadmium Selenide (CdSe), Cadmium Telluride(CdTe), Zink Selenide(ZnSe), Lead Sulfide(PbS), etc. QDs are also made from column III-V elements in the periodic table such as Indium Phosphide (InP), Gallium Nitride (GaN), Indium Arsenide (InAs) [16-20]. The Quantum Yield (QY) describe how QDs are efficient emitters. The QY is the ratio of the number of photons absorbed by the QD crystals to the number of photons emitted by the QDs. In other

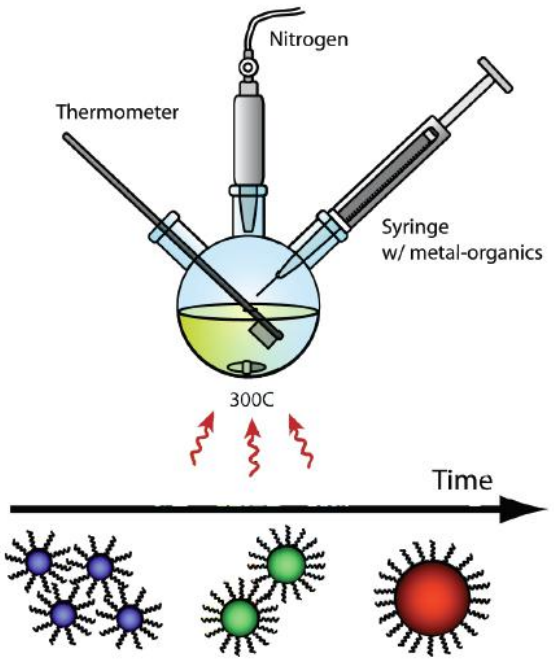

Figure 1.13 The schematic shows the QD synthesis in the three-neck flask. Organo-metallic precursors are injected into a boiling solution of organic molecules, that will eventually become QD ligands. The time scale indicates the growth progress [20].

words, QY is the probability of de-excitation only through radiative decays [16]. QDs can have a ligand layer (Figure 1.15) covering its core. This surface modification of QDs, ligands, is for surface passivation of QDs which leads us to increase the quantum yield up to 70%. The ligand layer must have a higher band gap energy than the core to order to prevent any interference with the emission of the QD cores and to not have any absorption of the emission. Additionally a ligand layer avoids carrier relaxation to the QD's shell [16-20].

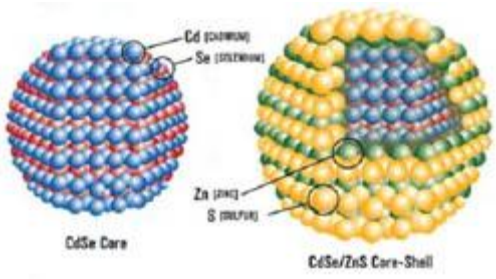

Figure 1.14 Core and core shell of a CdSe quantum dot the shell consist of zinc sulfide [20].

QDs have very many applications, including quantum computation, biology sensors, photovoltaic devices, and solar cells, light emitting devices, photo detector devices, fluorescence labeling, etc. [1-2].

1.13 Forster Resonance Energy Transfer (FRET)

Recent developments in bio-sensors and solar cells using colloidal QDs have increased interest in studying the interaction of colloidal QDs with each other. Colloidal QDs solids in close proximity support Forster Resonance Energy Transfer (FRET) to

generate energy flow from the donor to the acceptor via non radiative relaxation [16]. But certain conditions need to be met for this energy flow to happen. This mechanism occurs when dipole-dipole interaction between the QD's is possible. The probability of FRET can be calculated using equation 1.42 [16-21]

$$P_{DA} = \frac{R_0^6}{R_0^6 + R_{DA}^6} \quad , \tag{1.42}$$

where P_{DA} is the probability of electronic energy transfer R_{DA} is the distance between the donor and the acceptor and R_0 is a constant called the Forster radius. R_0 , equation 1.43, is the length at which the FRET efficiency is 50% and is typically 1-10nm [21].

$$R_0 \propto \left(\frac{\varphi_D}{n^4}\int_0^\infty F_D(\tilde{\nu})\varepsilon_A(\tilde{\nu})\frac{d\tilde{\nu}}{\tilde{\nu}^4}\right)^{1/6} \quad , \tag{1.43}$$

where φ_D is the quantum yield (QY) of the donor, n is the refractive index of the medium, $F_D(\tilde{\nu})$ is the normalized emission spectrum of the donor, and $\varepsilon_A(\tilde{\nu})$ is the molar absorption coefficient [16].

The integral in equation 1.43 represents the spectral overlap of the donor emission and the acceptor absorption; Where QDs have higher photoluminescent efficiency the probability of energy transfer increases.

In Figure 1.16 we can see the absorption and emission spectra for different sizes of QDs and Figure 1.17 shows schematic of FRET between donor and acceptor.

1.14 Optical Properties of Colloidal QDs

QDs have certain characteristics which make their use advantageous, when compared to commonly used fluorophores. This advantage is mostly due to the optical

properties of the QDs such as narrow emission spectra, high fluorescence quantum yield, wide excitation spectra, etc. Also the controllability of the luminescence properties is very important as quantum confinement will allow us to change the properties of the semiconductor nanocrystals by varying their size. One of the important factors in the quality of the QDs is their QY. The maximum value of QY is 1.0 (100%). In practice, even QDs with a QY on the order of 0.1(10%) are considered good fluorescent [16]. QY depends on the synthesis methods. Additionally, when QDs are in contact with a given environment, their QY will change. Depending on the type of environment (air, vacuum, substrate), the QY for various QDs can change significantly.

To explain why the environment has such a substantial effect on the QY of QDs, it is necessary to understand how relaxation processes happen once the absorption of photons has already brought the QDs to an excited state. In general when a photo-excitation happens an electron-hole pair is created. These excited carriers are then relaxed again via two major methods [16-22]:

- Radiative recombination
- Non-radiative relaxation

The radiative recombination takes place via the emission of a photon, bringing the excited state to the ground state

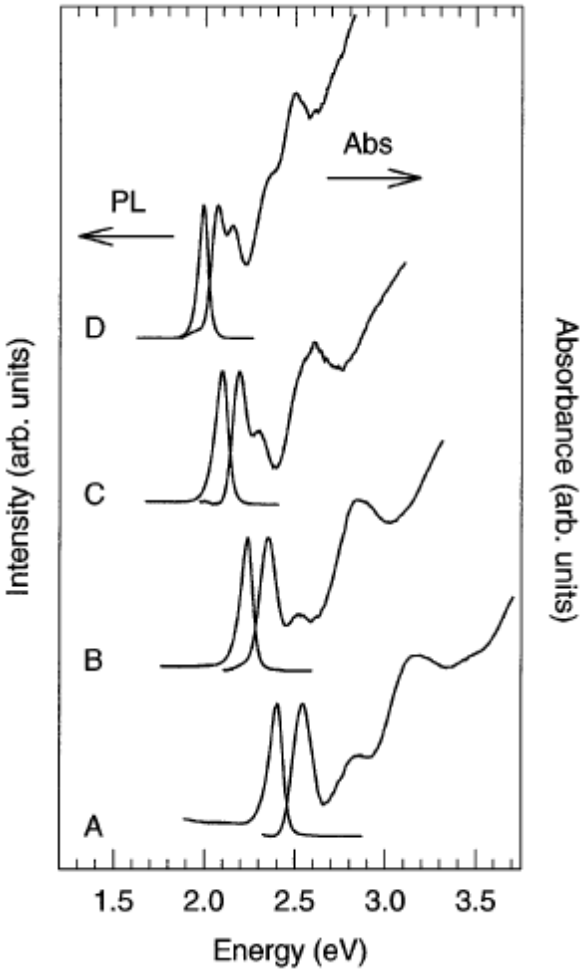

Figure 1.15 Optical absorption and photoluminescence spectra at 10 K of optically thin and clear, close-packed NC solids prepared from CdSe NC samples (A) 30.3Å, (B) 39.4Å,(C) 48.0Å, and (D) 62.1 Å in diameter (67) [16].

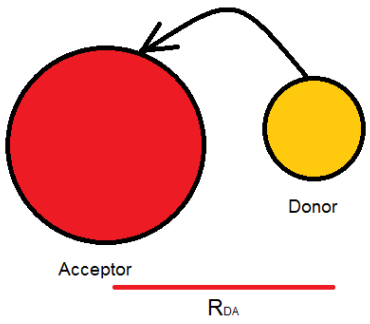

Figure 1.16 Sketch of FRET between donor and acceptor QDs.

This process determines the luminescence properties of the QDs. In the non-radiative method, QDs reach their ground states mostly through the entrapment of conduction-band electrons and holes in the surface traps. This type of relaxation leads to a reduction of the QY.

One accepted idea explaining the nature of this non-radiative process is the "long-lived trap hypothesis" suggested by Efros and Rosen [16-22]. Based on this hypothesis if a carrier (electron or hole) is trapped in the surrounding matrix, the energy relaxation in the QD happens mostly through a radiation-less Auger process. Since the time needed for the Auger process (~1 ps) is 3-4 orders of magnitude smaller than a radiation process time [16-22], the QDs won't have enough time to emit a photon and, therefore, the relaxation process will be dominated by the non-radiative process, reducing the QY significantly.

Surface imperfections can act as temporary surface traps for carrier and are one of the main sources of an increase in the non-radiative radiation and hence a reduction in QY is surface defects [16]. Therefore, the surface states of QDs is an important factor in the determination of the QY. However, there are many other reasons for a low QY, such as defects in crystal lattice, surface structures, and particle clustering. As a result, a lot of research other groups have been done to show the relation between the brightness, stability and the surface structure.

Clearly one of the most recognized methods for obtaining a higher PL is by the reduction of surface defects via surface passivation. There are many techniques for surface passivation of QDs. One way, as mentioned before, is to use a ligand (shell) with

a higher band gap energy than the core of the QDs. In such nanocrystals (core/shell), the excitation is restricted within the core of QDs because the electrons and holes prefer to fill the lowest energy state. However this type of design also reduces the chance of energy transfer in colloidal QDs because there are no electrons and holes available at the surface of QDs.[22]

1.15 Photo Fluorescence Enhancement (PFE) of QDs

When QD's are irradiated with light, their emission, efficiency increases due to a process referred to as PFE [22].

Many research groups are conducting different experiments for various QDs with different capping ligands to observe this photoactivation [22]. Clearly there are many different parameters that could be changed based on the specific setting of an experiment. Therefore comparisons of the results obtained by different groups are problematic. But in general their results show many common features including the increase of the efficiency of the QD's emission under illumination. Their results also show a blue-shift in the emission spectrum in the photoluminescence of QDs which is the sign of some evolution in QDs. This evolution indicates a decrease in size of QD core size during illumination [22].

It is commonly accepted that this photoluminescence enhancement is caused by surface modification of the QD's due to the removal of surface defects. However based on the passivation method used, PFE can be organized into different types. Using different types of surrounding medium can also lead to specific reorganization or reconstruction of the QDs.

1.15.1 PFE due to heat-induction by light (photoannealing)

When light impinges on QD nanocrystals, it is absorbed by the nanocrystals; however, some of the light beams are absorbed by the medium in which the QDs are embedded. Absorption of the light leads to an increase in the temperature of the QDs and medium surroundings, and the rise temperature induces surface reconstruction[22]. The surface of QD's is annealed by heat and light, via the removal of the loosely bounded Sc, Se or Te on the surface of CdSc, CdSe or CdTe, respectively, which act as hole traps. As a result of this removal of the unsaturated elements on the surface of QDs, we can remove some of the defects are removed from the surface of nanocrystals, leading to a higher QY for those QDs.

In the presence of nonpolar organic solvents such as toluene, surface annealing is the only method for photoactivation. With this method the emission spectrum of the QDs is not blue-shifted [22].

1.15.2 PFE due to adsorption of water molecules on the surface of QDs

This pathway is observed the in presence of O_2or N_2 and not in vacuum. Photoactivation with adjacent water molecules can be divided in two separate processes. At the beginning of illumination, the water molecules adsorb on the surface of the QD and passivate the surface from carriers traps increasing the photoluminescence of QDs. Also oxygen when is present in medium can cause acceleration in the photoluminescence activation [22].

1.15.3 PFE due to stabilization with surfactant molecule or surface-ligand passivation

Irradiation of light on nanocrystals causes photo-induction and rearrangement of molecules on the surface of QDs or the legands around the core of QDs. This process stabilizes/passivates the holes on the surface of Qds [22].

1.15.4 PFE due to photo-oxidation

Another method which can cause photoactivation is photo oxidation. For example, in CdSe/ZnS QDs, the surface Selenium atoms in CdSe QDs will be oxidized to selenium oxide during photo oxidation. The Selenium oxide molecules are removed from the surface of QDs, and the QDs becomes smaller so we expect to see blue-shift as well [22].

By the removal of these unsaturated bonds from the surface, the probability of the presence of carriers on the surface of QDs is increased which as a result causes an increases in the QY [2]. This phenomenon is observed even in the presence of a ZnS layer which indicates that oxygen is diffusing through the passivating layer. But the ZnS layer causes photo oxidation rate to decrease. This reduction is related to the thickness of ZnS layer which grows at the surface of the QD's core.

1.15.5 PFE due to Coulomb blockage

In a QD solid Coulomb blockage happens when an electron or hole in a QD solids injected to trap site outside of the QD. In this situation the electron or hole can have a long neutralization time. Neutralization time is the recombination time of the electron and hole via a radiati3ve or non-radiative process. Due to the charge of the ionized QD, we will have an electrostatic potential barrier is esteblished. This potential suppresses both

the slow and fast photoionization processes in the neighboring QDs. This process enhances the emission efficiency of such QD solids, causing PFE [23].

CHAPTER 2

EXTINCTION COEFFICIENTS CALCULATION FOR LSPRs

For applying LSPRs for our research we need to study optical properties of Metallic Nano Particles (MNPs). In this chapter we simulate absorption and scattering coefficients of MNPs with a numerical method to determine proper LSPR for our research.

2.1 Mie Theory

Mie Theory is the solution of Maxwell's equation for an electromagnetic wave that is scattered or absorbed by MNPs. Such processes (scattering and absorption) depend strongly on the size and shape of MNPs. To solve Maxwell's equation analytically it is necessary to apply the boundary conditions assume spherical shapes for MNPs. The equations are too c cumbersome to write down here, but the procedure to obtain them is fairly straightforward [24]. These equations can be generalized somewhat to more complicated shapes: ellipsoids, cylinders, concentric, etc. In general, the scattering and absorption coefficients vary as a function of both particle size and refractive index.

For simulating the optical properties (absorption and scattering) of spherical MNPs we used Mie theory. In this approach, the extinction. scattering and absorption cross section coefficients are expressed as [24]

$$\sigma_{ext} = \frac{2\pi}{|k|^2}\sum_{L=1}^{\infty}(2L+1)Re(a_L + b_L) \tag{2.1}$$

$$\sigma_{sca} = \frac{2\pi}{|k|^2}\sum_{L=1}^{\infty}(2L+1)(|a_L|^2 + |b_L|^2) \tag{2.2}$$

$$\sigma_{abs} = \sigma_{ext} - \sigma_{sca} \tag{2.3}$$

$$a_L = \frac{m\Psi_L(mx)\Psi_L{}'(x)-\Psi_L{}'(mx)\Psi_L(x)}{m\Psi_L(mx)\eta_L{}'(x)-\Psi_L{}'(mx)\eta_L(x)} \quad (2.4)$$

$$b_L = \frac{\Psi_L(mx)\Psi_L{}'(x)-m\Psi_L{}'(mx)\Psi_L(x)}{\Psi_L(mx)\eta_L{}'(x)-m\Psi_L{}'(mx)\eta_L(x)} \quad , \quad (2.5)$$

where $m=\frac{n}{n_m}$ and n is the complex refractive index of particle and n_m the real refractive index of the surrounding medium. k is the wave-vector of incident light and $x = |k|r$ which r is radius of MNPs. Ψ_L and η_L are the Ricatti-Bessel cylindrical function [24].

In the next section we apply dipole-dipole approximation to calculate these coefficients for MNPs which is much smaller than the incident wavelength.

2.2 Extinction Coefficients

In this calculation, our particles are much smaller than the incident light wavelength, and it can be shown that only the dipole oscillation contributes significantly [39] and we can apply this approximation in the Mie theory and calculate the total extinction cross-section of the metal which will consist of an absorption part and a scattering part [24]:

$$\sigma_{ext}(\omega) = 9\ \frac{\omega}{c}\varepsilon_{out}^{3/2}V\frac{\varepsilon_2(\omega)}{[\varepsilon_1(\omega)+2\varepsilon_m]^2+\varepsilon_2(\omega)^2} \quad . \quad (2.6)$$

In this equation V is the volume of the metallic nanoparticle and for the permittivity of the metal we have [24]

$$\varepsilon_{in}(\omega) = \varepsilon_1(\omega) + i\varepsilon_2(\omega) \quad . \quad (2.7)$$

As mentioned before, a metallic medium's refractive index has an imaginary part which will contribute to the absorption process. To make it clear how different materials

and their shape and size as well as the environment in which they are embedded in, can affect the extinction coefficient.

2.3 Modeling the Extinction Coefficients of a Nano Sphere

We have used a Mathematica code[14-25] which has an analytic solution for the Mie theory [42]. The extinction coefficient as a function of wavelength for a 40nm diameter sphere in vacuum with a refractive index of n=1, for gold (Au), silver (Ag), chromium (Cu) and Aluminum (Al) has been plotted in Figure 2.1.

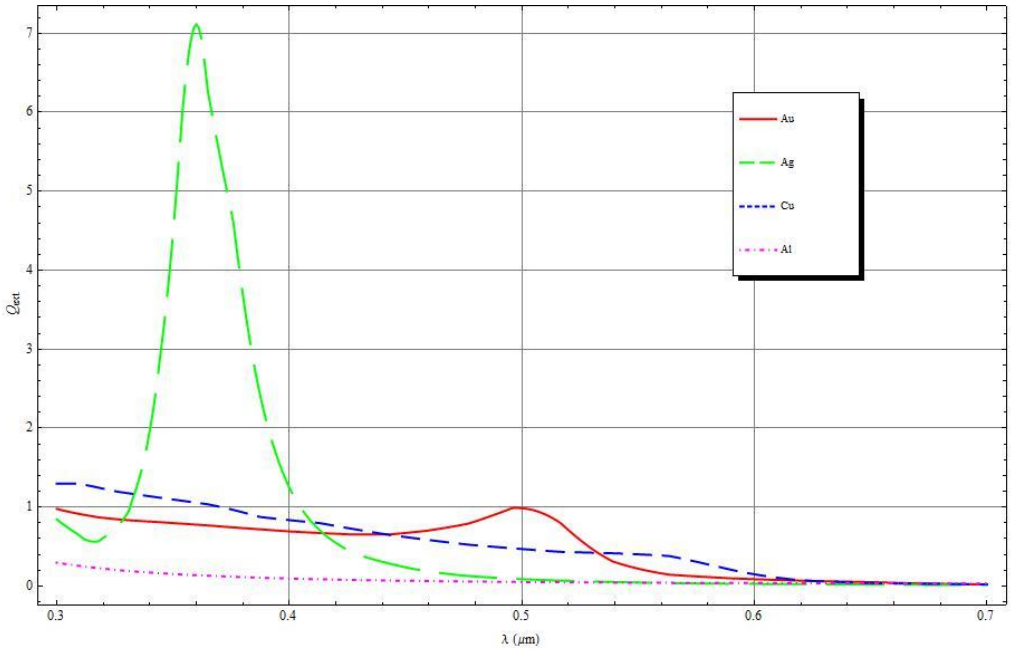

Figure 2.1 Extinction Coefficient as function of wavelength for different materials [14].

As you can see for this size of sphere, for different materials in Figure 2.1, silver shows better plasmonic behavior than the other materials and it has a sharp peak at 380nm wavelength. Gold also has a peak around 500nm wavelength. However, chromium and aluminum don't have a significant peak. Gold doesn't have a significant

peak at wavelength where it can give a high amplitude but chemically it is more stable than silver [14].

For biological sensors the materials must not be harmful to the human body; therefore, for sensor application researchers prefer to work with gold rather than silver.

In Figure 2.2 we plot the extinction coefficient versus the wavelength for a range of 40nm-400nm gold spheres in vacuum and show how the size of the nano-metallic particles can impact the plasmon frequency. As it can be seen in Figure 2.2, Plasmon

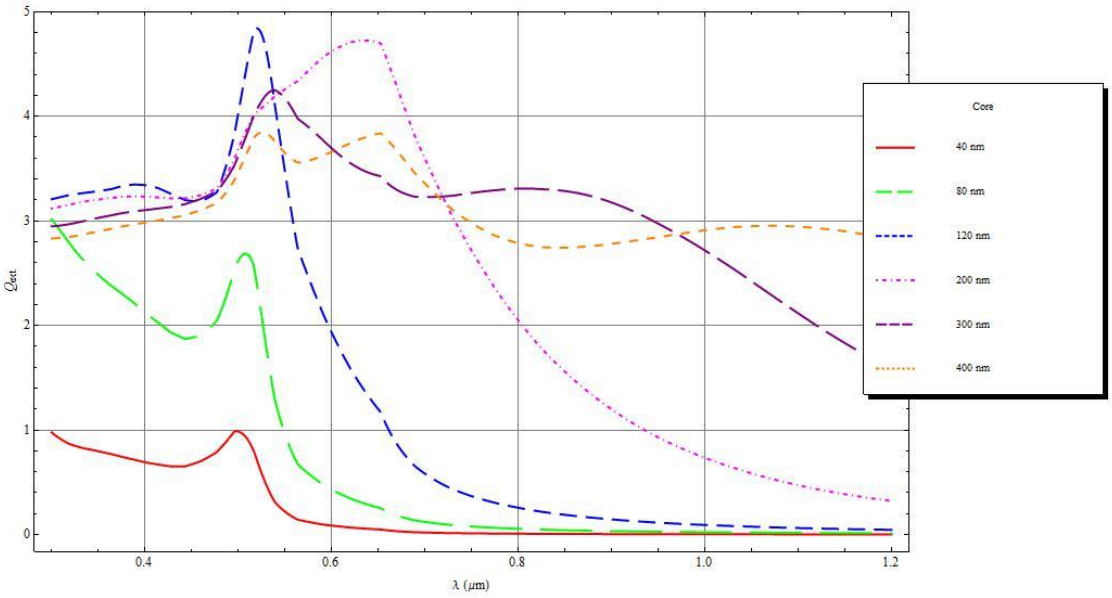

Figure 2.2 Extinction Coefficient as a function of wavelength for Au spheres of diameter 40nm-400nm.

frequency depends strongly on the size of the sphere. As mentioned before, the extinction coefficient is the sum of scattering and absorption coefficient and for sensing application.

It is crucial to know whether the scattering or absorption coefficients has a larger effect in the extinction coefficient since the scattering coefficient enhances the radiative decay of the florescence molecules in the neighborhood of the metal whereas the

absorption coefficient enhances the non-radiative decay of the fluorescence molecules. For the same conditions as in Figure 2.3 we can plot the scattering coefficient (Figure 2.4). Comparing Figure 2.3 with Figure 2.4 it can be seen that for small spheres, scattering coefficient is very low. For example, for a 40nm gold sphere there is no scattering field so the extinction coefficient which we see in Figure 2.3 is all due to the absorption coefficient.

Figure 2.4 shows that when particles become bigger, the scattering coefficients play a more important role in the extinction coefficient. For example, for a 200nm gold sphere the calculations indicate that more than 90% of the extinction coefficient is due to the scattering coefficient and the absorption coefficient plays a minor role.

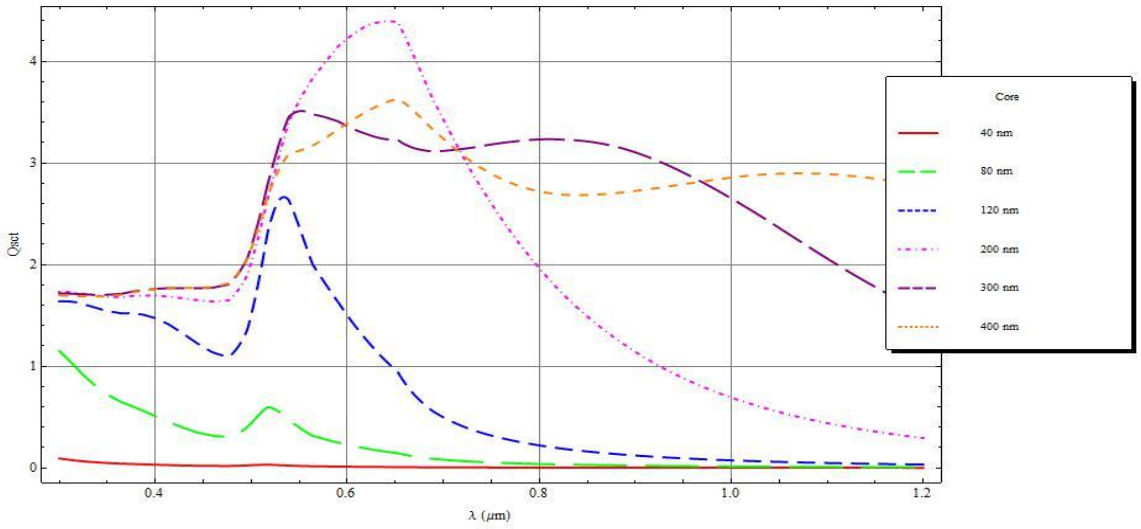

Figure 2.3 Scattering Coefficient as a function of wavelength for Au spheres of diameter 40nm-400nm.

Another important factor which can have an impact on the extinction coefficient is the environment which hosts our metallic nanoparticles, in general if our environment has a higher reflective index it can enhance the extinction coefficient and also cause a shift in the peak of the Plasmon frequency.

In Figures 2.4 and 2.5 the extinction and scattering coefficients are plotted respectively for a 40nm gold sphere which is embedded in a host dielectric material with refractive index n=1.0 to n=2.1. As can be seen in Figure 2.4, for a host with higher reflective index we have a large extinction coefficient and we have a red shift at the peak which is predictable from the Fresnel law.

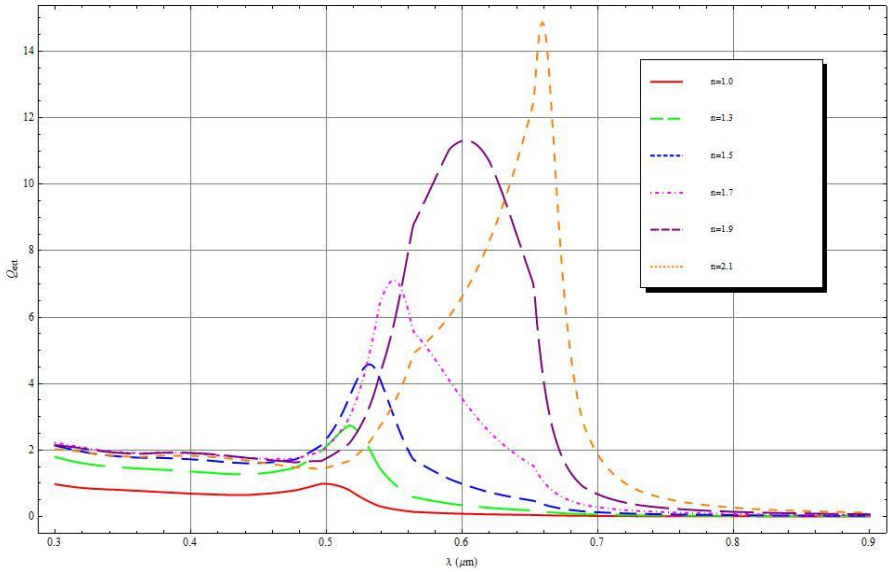

Figure 2.4 Extinction Coefficients as function of wavelength, for 40nm sphere of Au embedded in different dielectric.

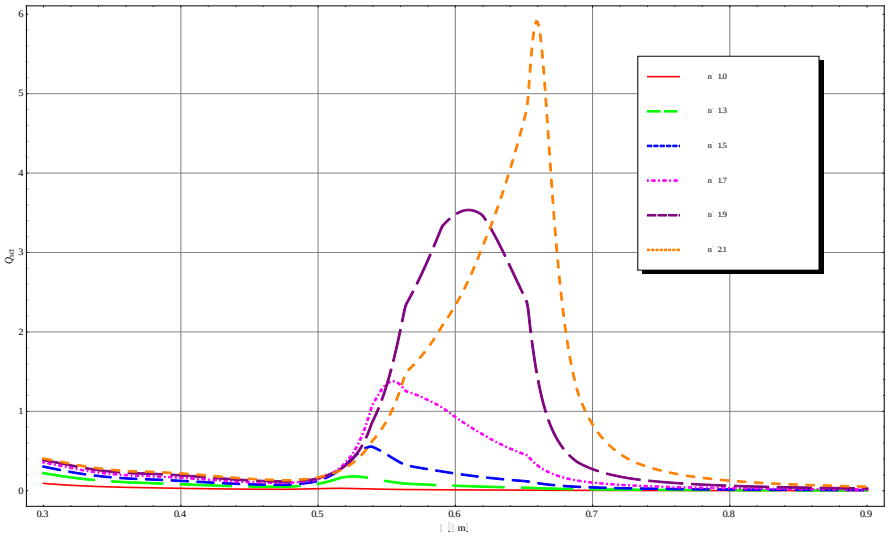

Figure 2.5 Scattering Coefficients as function of wavelength, for 40nm sphere of Au embedded in different dielectric.

Another influence of a higher reflective index medium is that the scattering coefficient undergoes a larger enhancement than the absorption coefficient (Figure 2.5). These graphs indicate that changing the environment can enhance the scattering field. All the parameters such as size, shape and environment are our tools to engineer a proper Plasmon peak for the desired application. For example for the fluorescence case if we want to suppress the emission of dye we can easily make a sample with nano-metallic particles with a higher absorption coefficients at a specific wavelength. Alternatively if we want to enhance the emission of dye we can engineer metallic nanoparticles with higher scattering coefficients in a specific wavelength that causes an enormous enhancement of the emission of dye.

Chapter 3 explains how to experimentally make metallic nanoparticles with different methods and use them in order to suppress or enhance emission of the quantum dots.

CHAPTER 3

SAMPLE FABRICATION AND OPTIMIZATION

Due to their exceptional optical properties such as wide range emission, high fluorescence efficiency, narrow line width, etc., QDs are promising candidates for application in sensors photovoltaic devices, solar cells, etc. [1-2]. In many of these applications, these nanocrystals are used in a closely packed configuration, forming two or three-dimensional QD solids. Recent studies have shown that these solids exhibit unique features when irradiated with light for a period of time. One of these unique features is a significant increase of their emission efficiencies (photo-induced fluoresce enhancement). Such enhancement has been attributed to various effects including passivation of the QDs' surfaces, photo-oxidation, thermal annealing and suppression of their photo-ionization rates.

In Chapter 2 we explained how Metallic Nano Particle (MNP) can have strong near fields. Such a field can enhance the photoluminescence of QDs. It can also enhance Forster energy transfer for various applications. These applications include sensing and diagnostic [1-2-8], development of optical and plasmonic devices, and enhancement of energy transfer between two different semiconductor nanostructures via plasmons. There have been many studies on the emission of thin film QDs excited by laser beams, both in the case when the QDs are in the presence or absence of MNPs. However, there has been no study on the dynamic of the emission of thin film QDs in the vicinity of MNPs when they are irradiated with a light. One of the main object of this study is to explore this QDs emission dynamic in presence of MNPs.

This chapter explains how the MNPs and samples are fabricated. The result of this investigation for the optimization of plasmonic enhancement of QDs and verifying impact of the scattering coefficient in enhancement are also presented.

3.1 Metallic NanoParticle (MNP)

In general different methods are used for preparing MNPs which results in three types of MNPs:

- Chemically (Colloidal MNP)
- Evaporation-Annealing
- E-beam lithography

Colloidal MNPs are prepared chemically and are embedded in a solution which is usually water [26]. The advantage of such MNPs is that you can spin coat them on a substrate. However, this technique leads to random distributions of QDs and we do not have much control on their separation. Also if we want to use colloidal MNPs due to the complicate process of their production, we need to buy an already made solution which is costly. As we need to study different shapes and sizes of MNPs many different colloidal MNPs need to be purchased since each solution has a specific size and shape of MNP.

In this investigation, evaporation-annealing and E-beam lithography methods are used to make MNPs. These methods provide more control on making MNPs in different shapes and sizes and also their separation from each other.

3.2 Evaporation-Annealing Method

The Evaporation-Annealing method was used to make gold (Au) MNPs on quartz (BK7) samples. The substrate (quartz BK7) is first cleaned with Xylene and Acetone and Methanol. Gold was evaporated onto the clean smooth quartz substrates at very low evaporation rate (0.1-0.2 Å/sec) in vacuum and with different thicknesses. The gold-coated quartz is then annealed in a furnace. Our data shows that the size and separation of gold nano particles after annealing are functions of the gold thickness, the annealing temperature, and time.

The motivation for using the evaporation method and not the sputtering method to deposition is that the sputtering method produce samples that are too uniform and smooth. This kind of smooth sample cannot result in MNPs. Figure 3.1 shows the differences in gold thin films when coated via an evaporation machine compared to when coated via a sputtering machine before annealing.

It is obvious from Figure 3.1 that the sample made via the evaporation method has dis-continuities and texture, whereas the sample made by sputtering is very continuous and smooth and we cannot see any texture on it. The formation dis-continuity is the basis for forming MNPs. Additionally as mentioned before, localized surface plasmon is function of size and shape of MNPs, and therefore, they can change significantly with any modification in structure. In addition, various localized surface plasmons can have different impacts on the photoluminescence of QDs which are of interest for us.

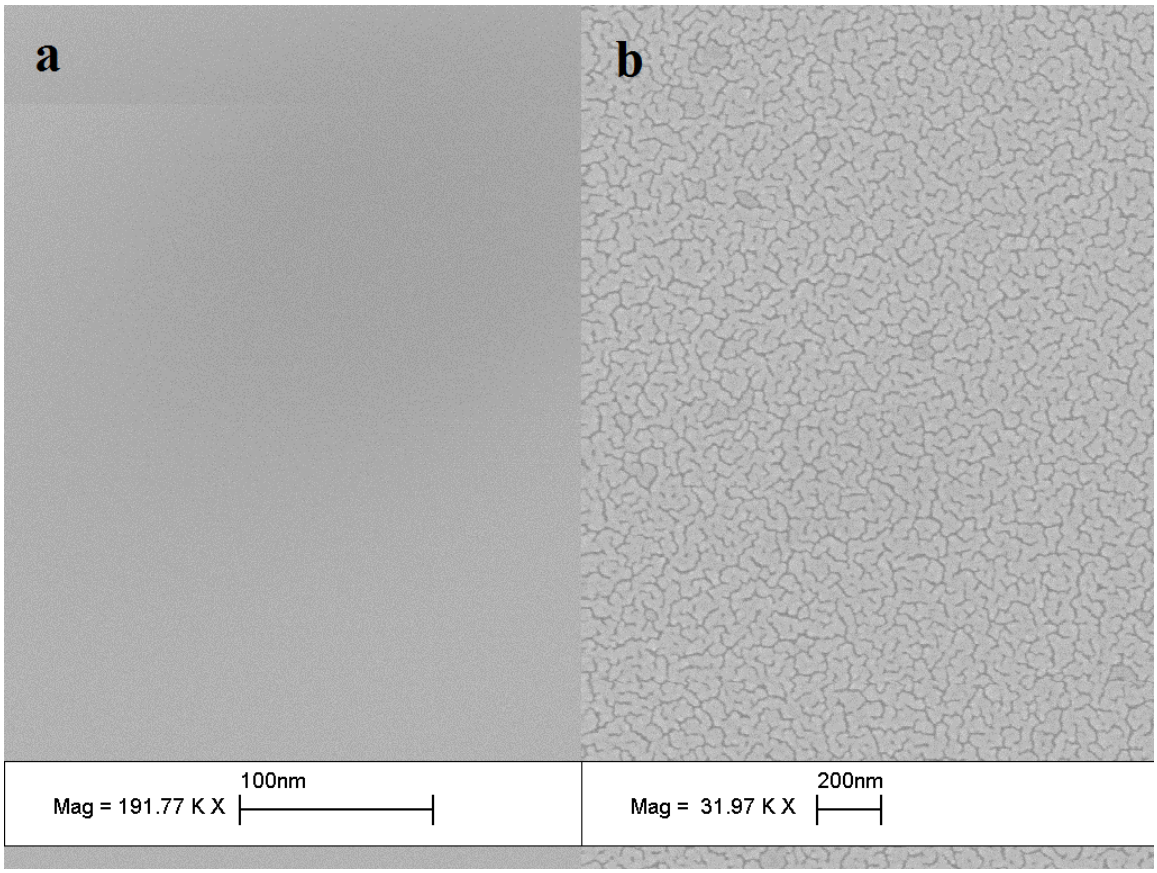

Figure 3.1 Scanning Electron Microscope (SEM) picture of gold (Au) 13nm thin film on quartz substrate which coated via (a) sputtering machine (b) and evaporation.

Gold thin films were evaporated on quartz substrate with thickness of 4,6,10 and 13nm. Samples were annealed for 30 min at 450℃, and then cooled.

In Figure 3.2 we can see Scanning Electron Microscopic (SEM) pictures of produced by different thickness of gold thin film when annealed under the same condition. The results show significant changes in the size of MNPs as the thickness of the thin films changed.

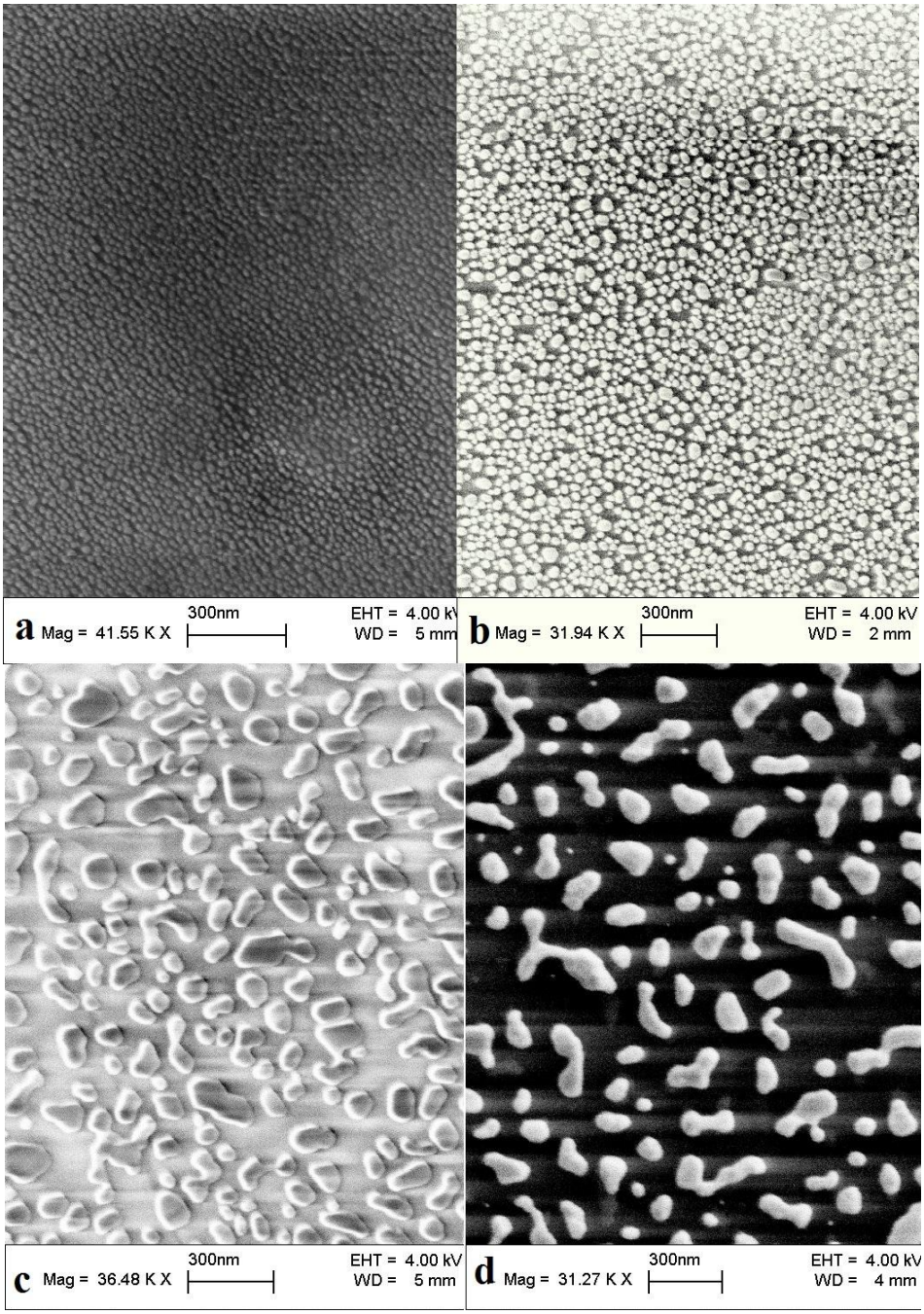

Figure 3.2 SEM pictures of gold thin film via evaportaion in vacuum enviroment after annealing in furance at 450℃ for 30 min , on quartz sample a) 4nm b) 6nm c) 10nm d) 13nm thickness of gold.

For example, the average size of the gold MNPs produced for a 4, 6, 10 and 13nm thin film were, 23, 41,100 and 150nm respectively. When the thickness of gold thin films increase, the shape of the MNPs becomes more random and non-uniform for the same annealing time and temperature. To solve this problem, the temperature and annealing time for each thickness of gold thin film was individually optimized.

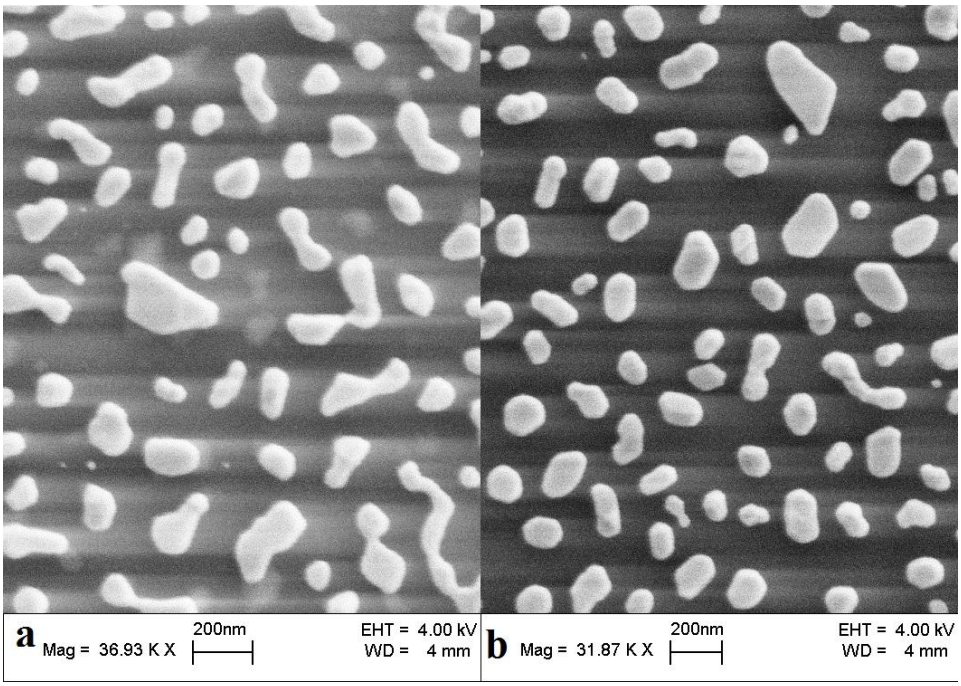

Figure 3.3 SEM picture of 13nm gold thin film on Quartz sample via evaporation a) Annealed at 450°C for 30 min b) Annealed at 500°C for 30 min.

In Figure 3.3, the SEM images of MNPs formed with 13 nm gold thin film with different annealing time and temperature are shown. It can be seen that with the increase of temperature, the MNPs become more uniform. For this, we change the furnace temperature from 450℃ (Figure 3.3-a) to 500 ℃(Figure 3.3-b). Comparing these two images, it is clear that MNPs in higher temperature are more similar to each other.

In general, the method described above is a very useful to make gold MNPs with feature sizes, ranging from 20nm to 200nm, very fast and with a low cost. However, this method is limited to forming MNPs smaller than 200nm. The reason is that when the gold thin film thickness is more than 15nm, the annealing does not give us MNPs, rather the films remain continuous. Moreover, with this method, the size of MNPs are more random and even after optimization (Figure 5.3-b) their shapes are not exactly the same, such non-uniformities in shape and size can lead to unexpected behavior in localized surface plasmsons. This is due to the strong dependency of LSPRs on the shape and size of the MNPs. To overcome this limitation the Electron Beam Lithography (EBL) method was used to make MNPs with desired shapes and sizes.

3.3 Electron Beam Lithography (EBL)

Lithography, in general, is a way of transferring a pattern. There are two different kinds of lithography to transfer patterns of a very small size, photolithography and E-beam Lithography (EBL). In Photolithography a photo sensitive resist is exposed to light in a similar way that photo films are exposed in photographic processes. Light goes through the transparency pattern in the photo mask and becomes focused on the resist via some optical component. With this method patterns are generate with feature sizes ranging from millimeters to a couple of microns. Creating pattern features with nano scale dimensions, require the resolution of an electron beam. In EBL, we use the electron beam of a SEM copies the pattern onto the sample coated with the resist. Since it is a serial process it takes much longer than a parallel process like photolithography.

For creating patterns with EBL, we used the NPGS software to generate a “design CAD file” for the desired pattern. This file was then used to control the SEM.

The substrate for the EBL samples was cleaned using the same method as for the evaporation- annealing method. After that we spin coat E-Beam sensitive resist (ZEP520A) onto the substrate. The thickness of the resist layer on the substrate can be controlled by changing the viscosity of the resist and also the speed at which it spins coated. After the spin coating of the E-Beam photo resist we need to bake it for 30 min at 120℃ for it to become ready for writing. After our samples are ready for writing we put them in the SEM chamber and use the NPGS software to write the desired pattern on them, as can be seen in Figure 3.4.a. After the writing we put our samples in a solvent to develop it. In the developing process the area illuminated by electron beams will be removed by the resist developer shown in Figure 3.4.b. To make the MNPs, we use an evaporation machine to coat gold onto the developed substrate as can be seen in Figure 3.4.c. In the final step, we need to remove all the resist which has remained on the substrate using resist stripper. At the end, our substrate has the desired pattern with the selected metals which we evaporated on the sample.

Additionally as mentioned before Localized Surface Plasmon Resonance (LSPR) are strongly dependent on the shape and size of MNPs, therefore With the EBL method, we are able to create the exact size and shape of MNPs which we are looking for. As we shown in Figure 3.5 with this method, we were able to create different patterns with feature size larger than 100nm. We used some of these patterns to investigate the emission of QDs in proximity to MNPs.

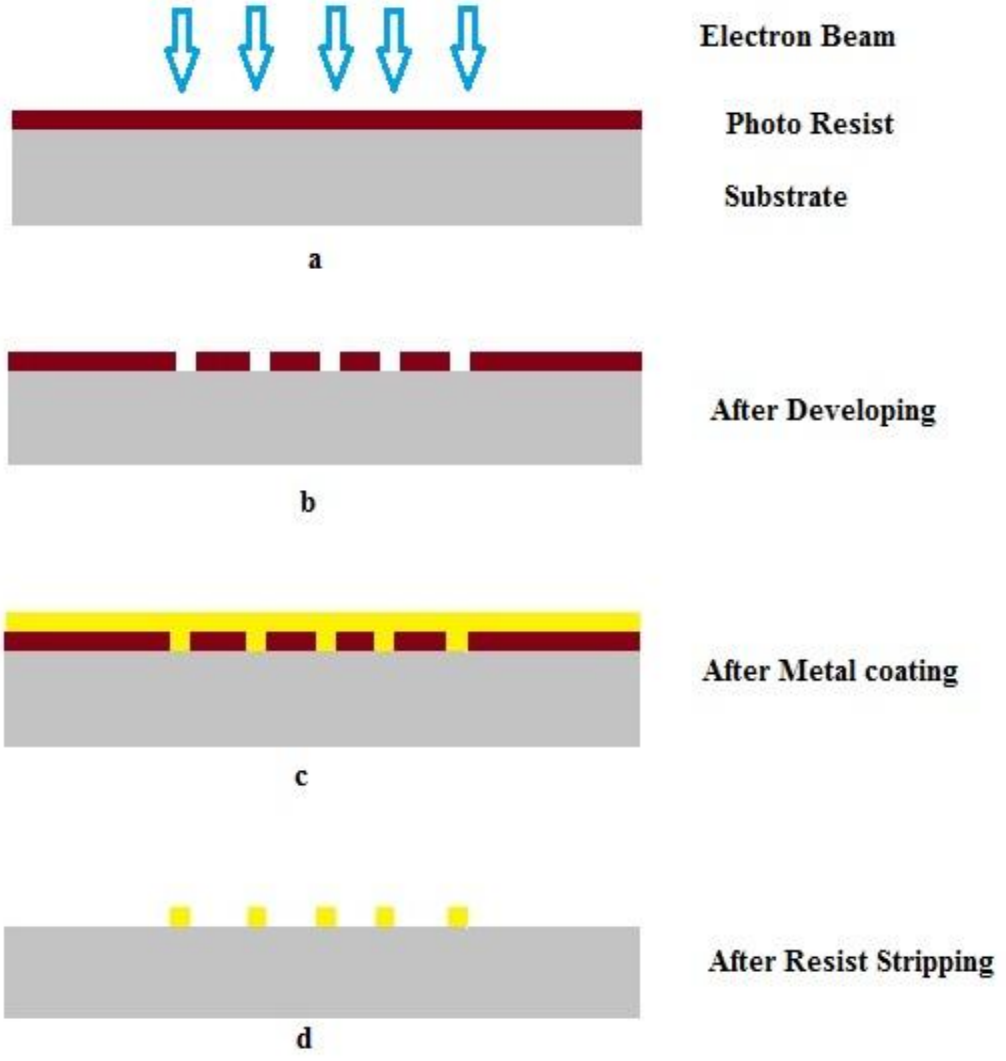

Figure 3.4 E-Beam lithography process a) prepared substrate after resist coating and baked, illuminated by electron beam b) resist removed by resist developer in illuminated area by electron beam c) gold deposition by evaporation on developed sample d) Stripping the remained resist on the substrate by resist stripper.

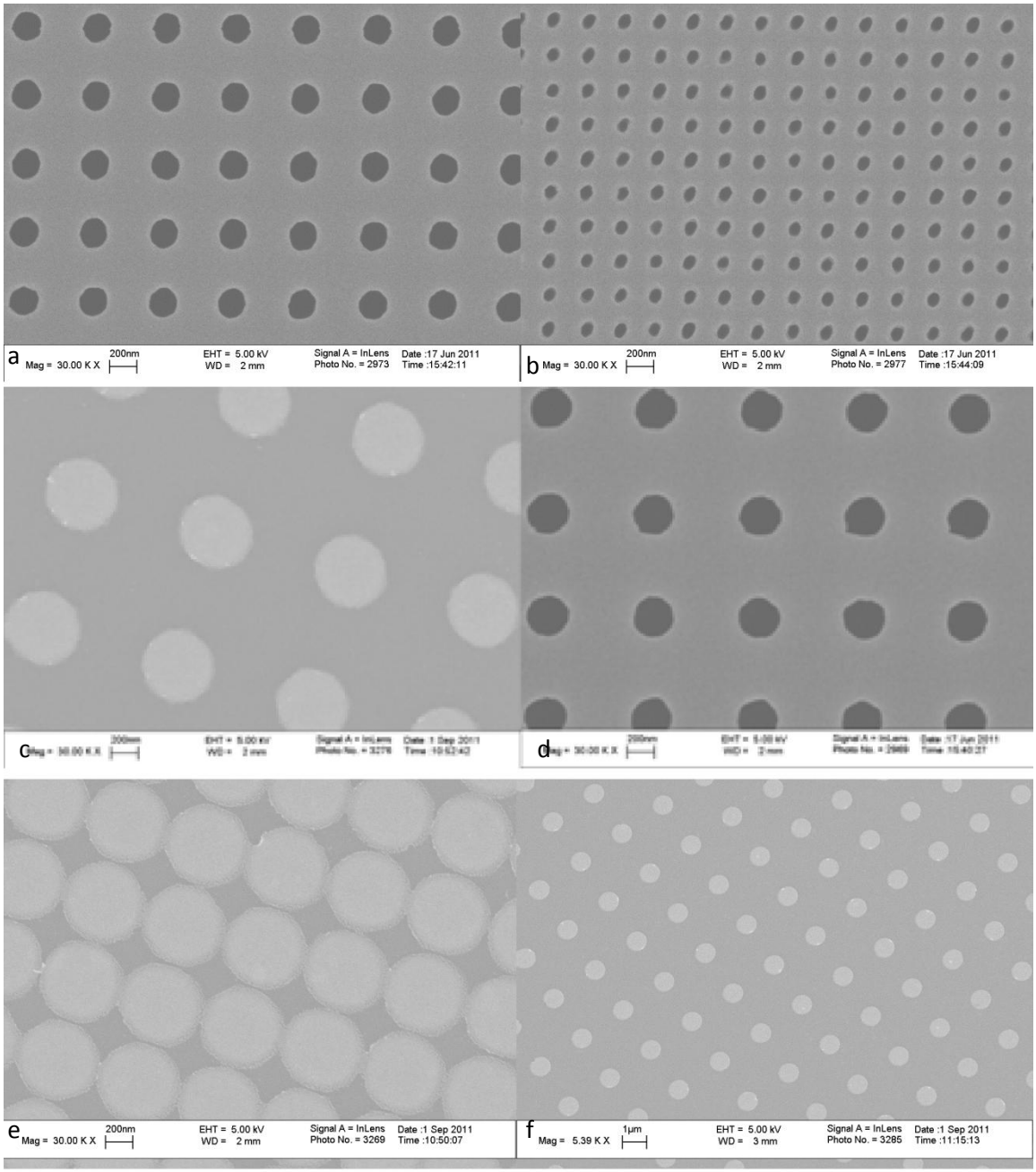

Figure 3.5 SEM picture for 50nm thickness gold nano disk with (a) 200nm diameter and 500nm separation (b) 100nm diameter and 300nm separation (c) 400nm diameter and 1$\boldsymbol{\mu m}$ separation (d) 200nm diameter and 700nm separation (e) 400nm diameter and 450nm separation (f) 700nm diameter and 2$\boldsymbol{\mu m}$ separation.

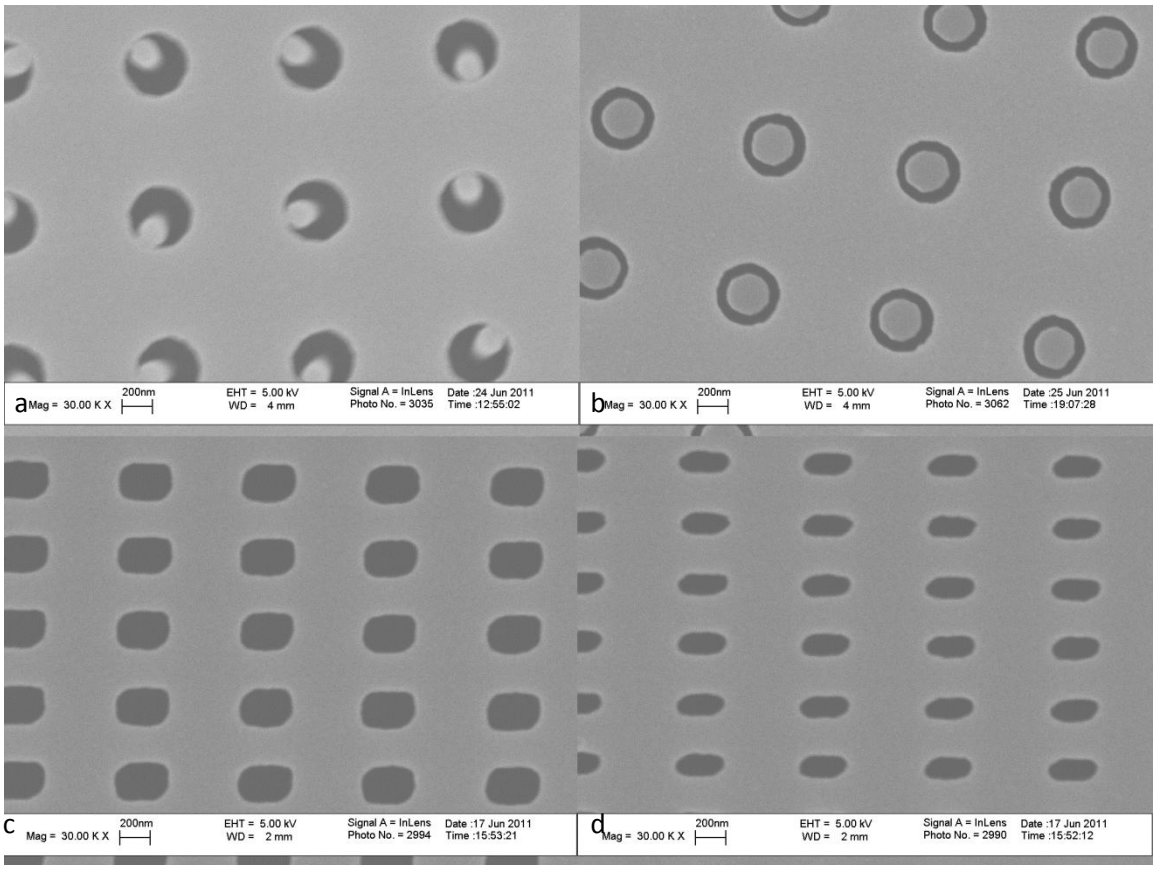

Figure 3.6 Figure SEM picture for 50nm thickness gold (a) nano crescent mask with 400nm diameter (b) 50nm nano rings mask (c) and (d) nano rectangular gold shape.

3.4 Emission of QD Solids in Presence of MNPs

The discussion in Chapter 2 showed that MNPs can enhance the electric field in their vicinity. In Chapter 1 showed that how the QDs emission can be manipulated by the environment due to the heat, oxidization, etc.

In this section we study the effect of localized surface plasmon resonance (LSRP) of MNPs on QDs emission is discussed.

3.5 Experimental Measurements of LSRP of MNPs

A spectrometer and white source were used to measure the plasmonic absorption peak of our samples with 4, 6, 10 and 13nm gold which were annealed at 450℃ for 30min. Figure 3.7 shows the plasmonic absorption peak of the MNPs sample produced by the Annealing - Evaporation method.

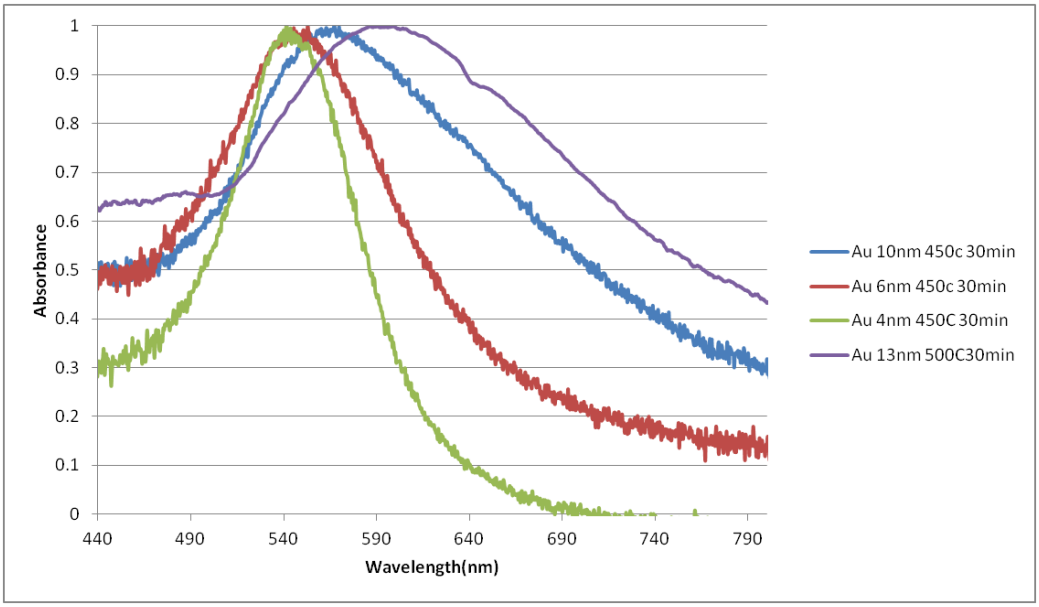

Figure 3.7 The absorption spectra of Au NPs for different thicknesses of gold thin film, green line representing 4nm; red line representing 6nm; blue line representing 10nm; and violet line representing 13nm Au thickness with Annealing condition of 450°C for 30 min for all samples.

These results suggest that by increasing the size of MNPs, the absorption plasmon peak spectra show a red shift and simultaneously their full width half maximum (FWHM) increase. These results agree with our numerical calculation for the extinction coefficient

of single spherical MNP. Which showed the extinction coefficient undergoes a red shift when the metallic particle become bigger.

For our research we studied variation of QD solids emission in presence of plasmonic effect. As the first step, we needed to fabricate samples consisting of MNPs and colloidal QDs separated from each other by a given distance. We evaporated 4,6,10 and13nm gold on glass substrates then anneal them in same temperature and time. This led to formation of nano island with different size as we explained previously. After the annulment we should put some space layer on top of the gold, to be able to control the range of the space layer, so we sputtered 15nm SiO2 on our MNPs samples. After that we spin coated CdSe/ZnS(625nm) colloidal QDs were obtained in toluene solution from NN labs, LLC., on MNPs samples. Figure 3.8 [27] shows the emission and absorption spectrum of CdSe/ZnS which we used in this experiment.

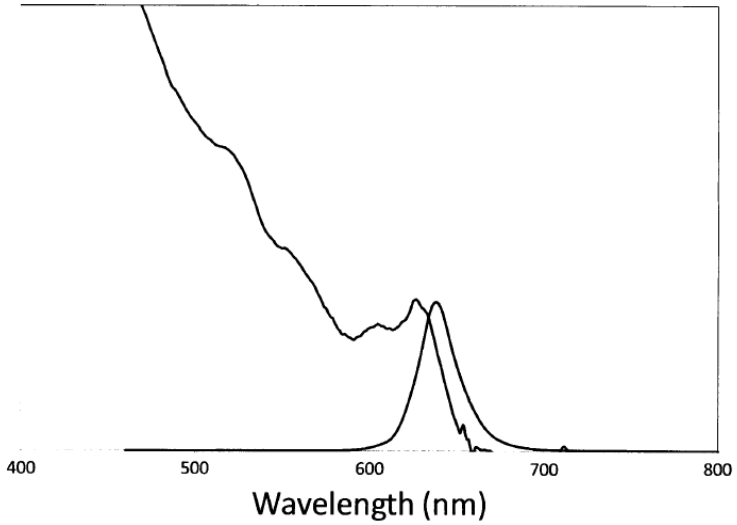

Figure 3.8 Absorption and emission specrum of CdSe/ZnS QDs [27].

We illuminate our samples with an Ar ion laser (514nm) perpendicular to their planes. We use the microscope objective to focus the laser beam to 400um beam size and to collect of the QDs emission. The dichroic mirror was used to direct QDs emission to a thermoelectrically cooled spectrometer where the spectra of the QD emission were recorded. Figure 3.9 shows the schematic of this setup.

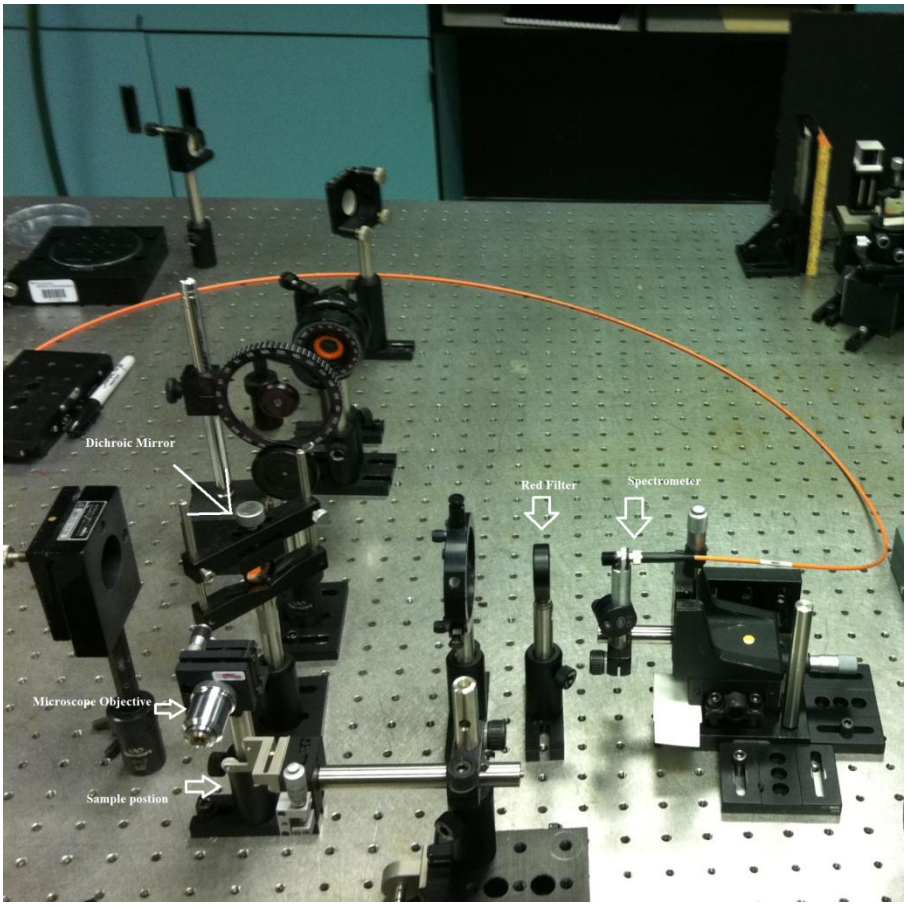

Figure 3.9 Lab setup picture.

The spacing between the plasmonic structure and the luminescent material and also the size of metallic nanoparticles affect the balance between the quenching and enhancement mechanisms. Figure 3.10 shows how the separation layer plays role on optimization process. These results show that for 15nm thick SiO2 layer the field

enhancement of plasmons actually dominates the FRET from the CdSe/ZnS QDs to the nano-islands.

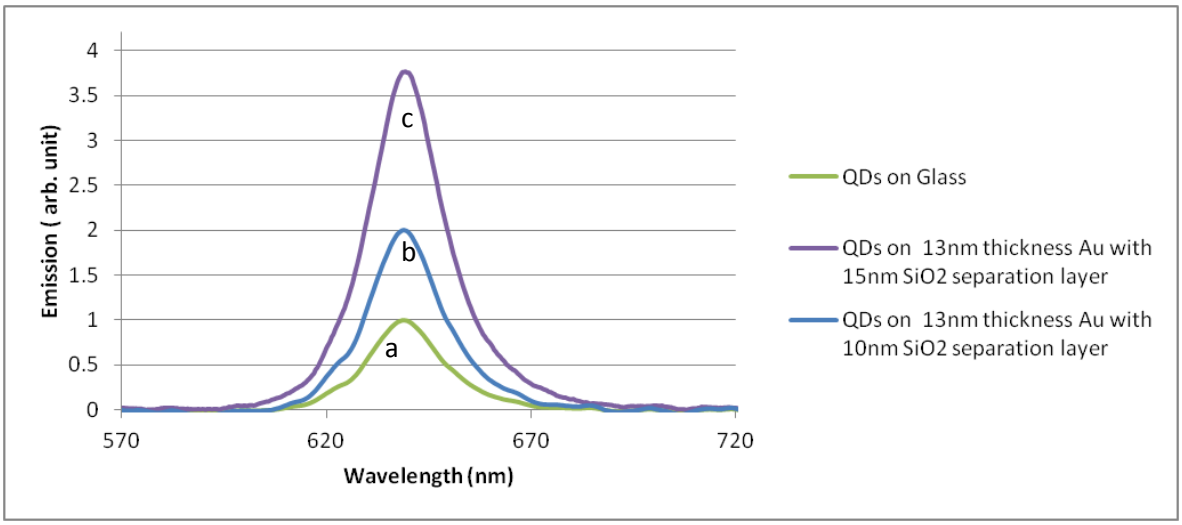

Figure 3.10 Peak emission of CdSe/ZnS QDs on glass (a) on gold with 10nm separation layer (b) on gold with 15nm separation.

Now we find that for our case 15nm separation layer is the best distance to have most plasmonic photo-luminescence enhancement in QDs emission. So we need to optimize the MNPs by variations of evaporation thickness on substrate.

Figure 3.11 shows emission of QDs in presence of different MNPs size samples. The enhancement or suppression in emission of such QDs on our samples represents the effect of plasmon field of different MNPs. When the thickness of evaporated layer of gold decreases or when we are dealing with very small the metallic nano-islands, the QDs' emission shows a dramatic suppression. This is due to the fact that for the small MNPs the extinction absorption coefficient of LSPRs is higher than scattering extinction coefficient.

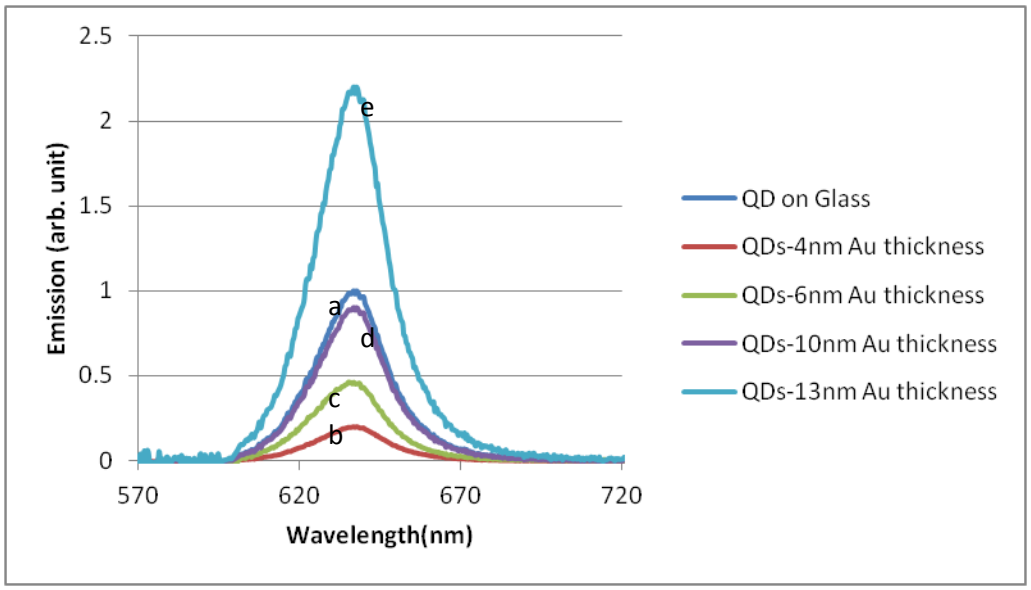

Figure 3.11 Peak emission of CdSe/ZnS QDs (a) on glass (b) 4nm Au thickness (c) 6nm Au thickness (d) 10nm Au thickness (e) 13nm Au thickness.

Therefore, the non radiative decay emission of QDs will be enhanced, which leads to the observed suppression in intensity. Our calculation in Chapter 2 shows that the smaller nano islands are, the more absorption extinction coefficient they have. So we expect to see more emission enhancement on bigger nano island because of the bigger scattering coefficient it has. A proper optimization of the nano-islands sizes and shapes and the separating layer thickness, leads to significant emission enhancement of the CdSe/ZnS QDs.

Figure 3.12 shows the optimized of samples with MNPs formed with 13nm of gold evaporated and 5optimization results of the temperature and annealing time for 13nm evaporated samples which we had most enhancement on. The optimal annealing parameters for 13nm gold thin film are 500℃ temperature and 30min of annealing time. The amount of emission enhancement has increased by a factor of 3.7.

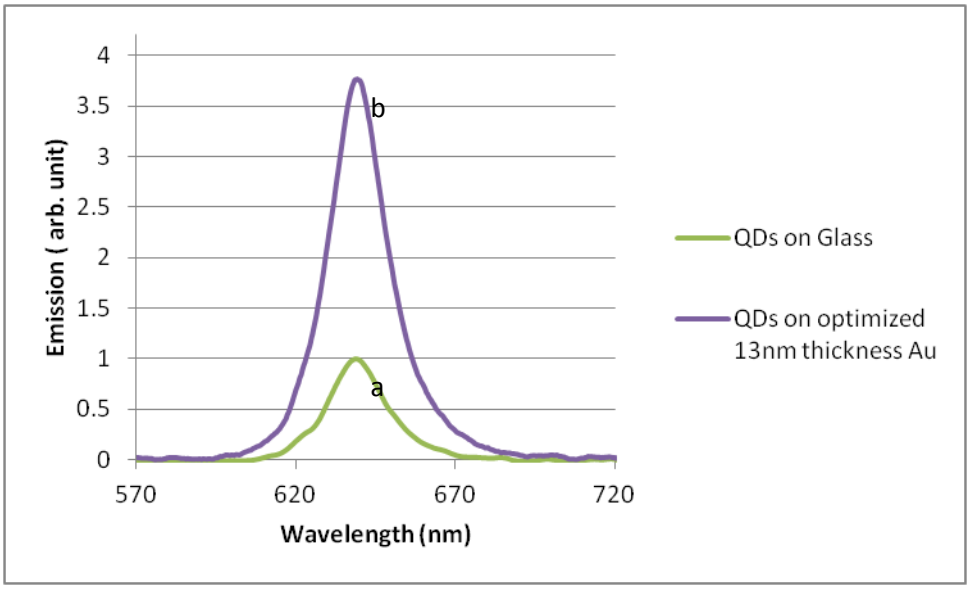

Figure 3.12 Peak emission of QDs (a) on glass (b) optimized 13nm Au thickness.

We improved the QDs' emission enhancement by a factor of 3.7 due to the stronger plasmonic filed that we obtained with the optimized Evaporation-Annealing method compared to QDs emission without MNPs on glass sample. Further emission enhancement by metallic nanoislands was limited because of their random sizes and shapes.

EBL method in contrast to the Evaporation-Annealing technique gives us the opportunity to produce desired sizes and shapes of MNPs. CdSe/ZnS QDs' emission in presence of 400nm diameter gold nano disk with separation of 1μm and with 50nm thickness (Figure 3.5.c) shows near to 7 times emission enhancement. This is almost 2 times more than the emission enhancement with optimized sample produced by evaporation method for the same type of QDs.

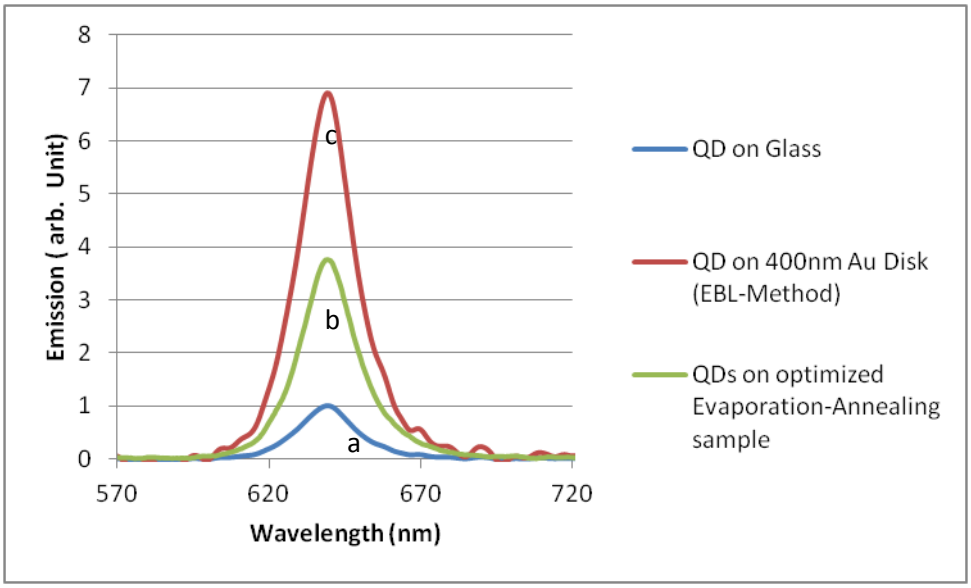

Figure 3.13 Peak emission of CdSe/ZnS QD's (a) on glass (b) optimized with Evaporation-Annealing methodb) on 400nm gold disk with EBL method.

In theory, we are able to design and create the pattern of MNPs which produce the desired LSPRs with the EBL method. And with proper LSPRs we can enhance emission of QDs significantly and even change the order of magnitude of the QDs' emission which it is very crucial for sensing applications.

Chapter 4

RESULT AND DISCUSSION

In this chapter we study thin emission of thin film QDs solid (CdSe/ZnS) in the vicinity of MNPs. For this we investigate variations of both intensity and spectra of such thin films with time and the intensity of laser. Our results show that at a given intensity of our laser the plasmonically enhanced emission of such solids starts to decline abruptly, making them inefficient emitters. In addition, for studying the QDs emission in vicinity of MNPs we study effect of heat which is generated by MNPs on QDs spectra [28].

4.1 Field-dependent Emission of Quantum Dot Solids

We explored the field-dependence of quantum dot solids when there are close to MNPs. To do so, we fabricated gold metallic nanoparticles (MNPs) on a glass substrate and covered this with 15nm of SiO_2, an optimal spacing are obtained for maximum enhancement of the CdSe/Zns core/shell Quantum Dots (QDs). 13nm of gold evaporated on the substrate and then annealed at 500℃, the evaporated gold gathered into nanoparticles had plasmonic absorption peak be around 570nm. All samples with QD solids were irradiated using a 514nm argon laser perpendicular to the substrate surface through a microscope objective. The objective collected the light emitted from the QDs which was directed toward a thermo- electric spectrometer using of a dichroic mirror. The full-width half-maximum (FWHM) and intensity of the resulting QD emission spectra were measured for various intensities of laser for the areas of the sample with and without MNPs were obtained and compared .

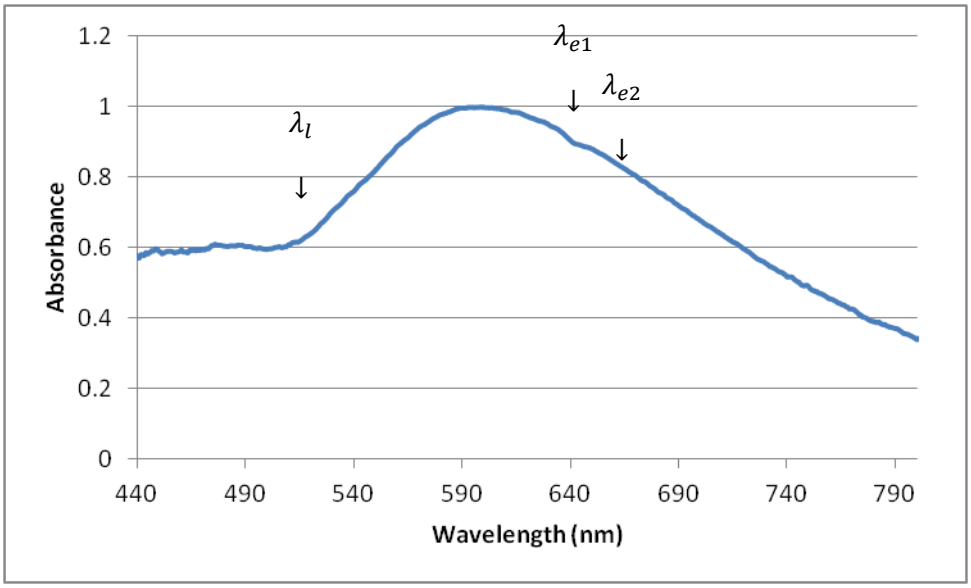

Figure 4.1 The transmission spectrum of MNP sample. $\boldsymbol{\lambda_l}$, $\boldsymbol{\lambda_{e1}}$ and $\boldsymbol{\lambda_{e2}}$ refer, respectively, the laser and QD#1 and QD#2 emission peak wavelength.

We used two types of CdSe/ZnS QDs with emission wavelength at 639nm (QD639) and emission wavelength at 655nm (QD655). We found that in the absence of MNPs, the peak of the QD emission spectra as well as the FWHM varied little as the laser intensity was increased. However, in the areas where the MNPs were present, 9nm and 12nm red shift in the peak spectral values of QD639 and QD655 respectively were observed as well as a 13nm and 20nm FWHM increase in QD639 and QD655 spectra respectively (Figures 4.2 and 4.3). This suggests the occurrence of greater than 60% broadening enhancement in FWHM of QDs spectra. The emission intensity of QDs in the absence of the MNPs was found to be linear with increasing of the laser intensity. However, in the presence of MNPs, the QD peak emission was found increased with laser intensity fairly linear, until it reaches a maximum value and then falls abruptly (Figure 4.4.c).

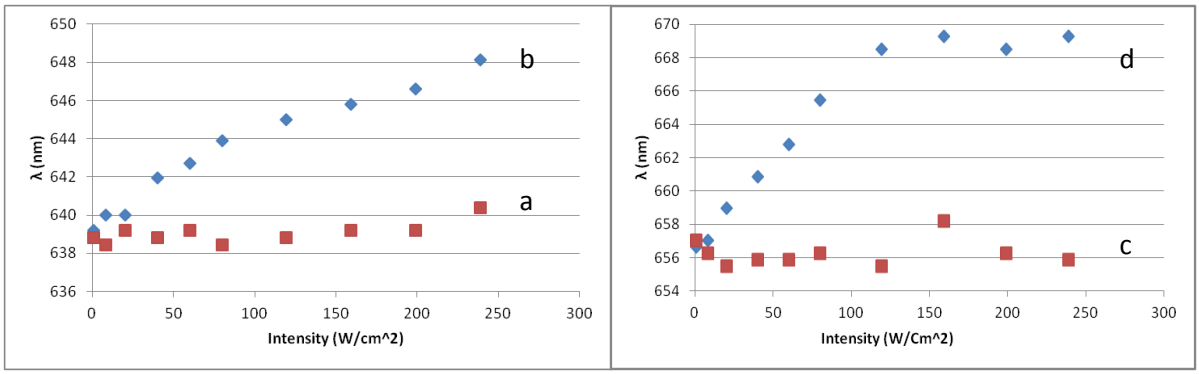

Figure 4.2 Variation in the emission wavelength of the QDs with (a) 639 nm emission (c) 655nm emission wavelength as a function of the laser intensity in the absence (red square) and presence (blue square) of MNPs, (b) QD639 and (d) QD655.

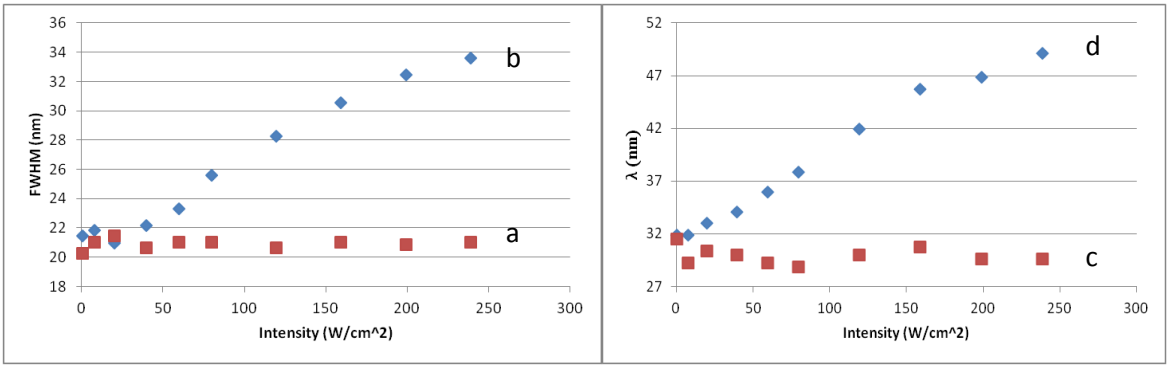

Figure 4.3 Variation in the FWHM of emission spectra of the QDs with (a) 639 nm (c) 655 nm emission wavelength as a function of the laser intensity in the absence (red square) and presence (blue square) of MNPs,(b) QD639(d)and QD655.

This result suggests the abrupt activation of non-radiative decay rates of QD solids due to the presence of the MNPs. These results also suggest that though QD enhancement; peak emission intensity of QDs in presence of MNPs compare to peak emission intensity of QD in absence of MNPs; depends strongly on the laser intensity in the presence of MNPs (Figure 4.5).

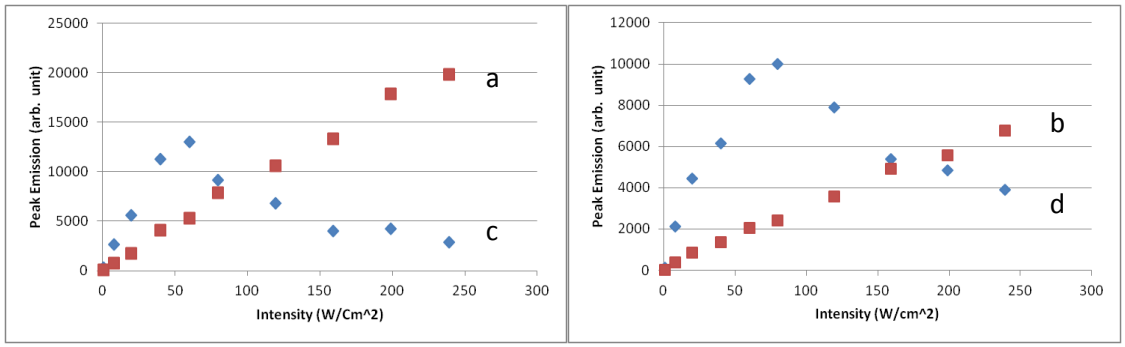

Figure 4.4 Variation in the emission peaks as a function of the laser intensity. Here the red square refers to (a) QD639 (b) QD655 emission in the absence of MNPs and the blue square refers to the emission of (c) QD639 (d) QD655 in the presence of MNPs.

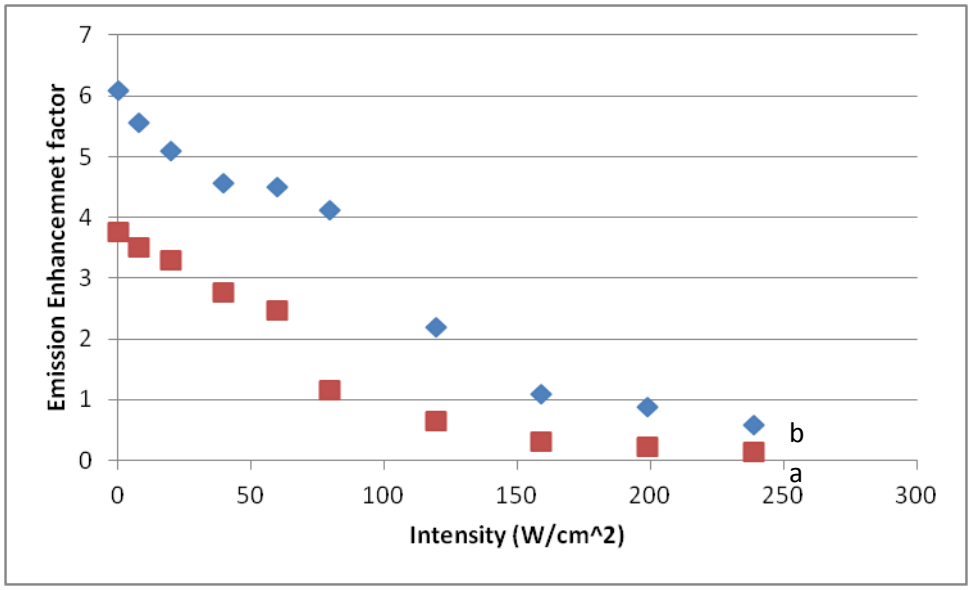

Figure 4.5 Variation in the plasmonic emission enhancement factors as a function of the laser intensity for (a) QD 639 and (b) QD655.

4.2 Plasmonic Effect on the Emission of QD Solids

To understand the nature of the abrupt change in QDs' emission in presence of MNPs, we need to explore the effect of plasmonic field enhancement and FRET. In addition, MNPs can absorb the laser beam and generate heat. We need to study the effect of the heat which generated by MNPs and effect of heat on QDs solids emission.

To study effect of field enhancement of MNPs we need to define $P_{enh}(\omega)$ [28]:

$$P_{enh}(\omega) = \left|\frac{E_{plas}}{E_0}\right|^2 \quad . \tag{4.1}$$

Here E_{plas}refers to the field in the vicinity of MNPs, and E_0 to the field in the absence of the MNPs in the same location. Such a field enhancement can also lead to the enhancement of the carrier excitation, depending on the frequency of the exciting light source (laser field). Therefore, in principal, E_{ehn} is influenced by the field enhancement at both the laser and QD emission wavelengths.

This abrupt change in the QD emission in the presence of the MNPs is controlled by the plasmonic field enhancement due to the MNPs, the heat generated by the MNPs, and photo-excited carriers.

First of all, the plasmonic enhancement of the QD emission depends on Forster Resonance Energy Transfer (FRET). Such field enhancement is a function of the frequency of the exciting light source, and it can result in the enhancement of carrier excitation. To summarize, the resulting enhanced field is a consequence of the individual enhanced fields of the laser and QDs at their respective emission wavelengths. According to our numerical calculation in chapter 3and other groups results [29], plasmonic field

enhancement reaches a maximum value at wavelengths larger than the plasmonic absorption peaks. In our experiment excitation wavelength is 514nm which is located in shorter wavelength of plasmonic field. Since scattering extinction coefficients which could lead to the enhancement of the carrier excitation, are located at longer wavelength side the plasmonic absorption peak as we shown in Section 3.5. Therefore we expect to see significant emission enhancement. As we have seen in Figure 4.5, QD639 peak emission enhanced 4 and QD655 enhanced 6 times.

Due to the high field intensity in vicinity of MNPs, initially we study the peak emission of QDs in very high power intensity to explore the impacts of high carrier excitation. Placing a thin film of QDs on a glass substrate, we observed the emission of the QDs mentioned above in the absence of MNPs at various irradiation intensities. The emission increases linearly with the laser intensity then rolls off at around 3000 W/cm^2 (Figure 4.6). This "roll off" is due to the heat caused by the excess release of energy of photo-excited carriers and Auger nonradiative decay. Overall, a red shift of less than 3nm; thus, we may ignore the impact of the carriers.

For having more comprehensive view of QDs emission in vicinity MNPs, we study effect of heat on QDs emission spectra in following.

After that we study QDs emission as a function of time to find out PFE factors which contribute in dynamic emission of QDs in and absence of MNPs.

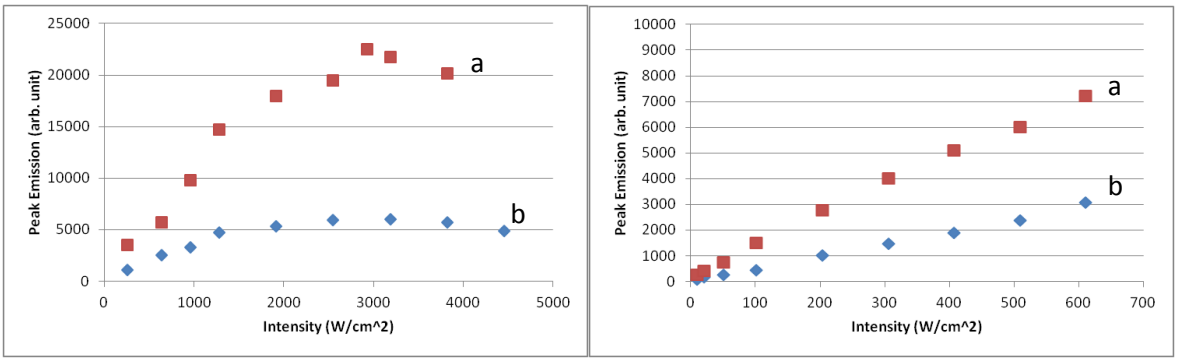

Figure 4.6 Variation in the peak intensity of the (a) QD639 (b) QD655 solid in the absence of MNP as function of laser intensity.

4.3 Heat Generated via MNPs

MNPs due to the high absorption coefficient σ_{abs} in their plasmonic peak frequency absorb irradiated laser and generate heat around the particles.

We consider gold MNP spheres of radius "a" arranged in a two-dimensional array embedded in a silica matrix with spacing Δ. The QDs are placed atop the matrix at a distance of R=15nm from the top of the MNPs. First we will discuss how the heat generated by the MNPs manipulates the QDs' emission. Then all other processes which affect enhancement will be discussed.

We study temperature changes in MNPs when they are irradiated via the Argon laser. According to reference [30] we can calculate ΔT as follows:

$$\Delta T = \frac{\Delta T_s a \sqrt{N_{MNP}}}{\Delta} \quad . \tag{4.2}$$

ΔT_s is the temperature increase at the surface of an isolated MNP. In this calculation we consider a single MNP which is embedded in silica matrix. For a single MNP the temperature rise is [28]

$$\Delta T(r) = \Delta T_{MNP} \frac{a}{r} \quad r > a \qquad . \tag{4.3}$$

$$\Delta T(r) \approx \Delta T_{MNP} \quad a > r \qquad . \tag{4.4}$$

ΔT_{MNP} is given by

$$\Delta T_{MNP} = \frac{Q_{MNP}}{4\kappa\pi a} \qquad , \tag{4.5}$$

where Q_{MNP}, is the heat generation rate in the MNP and I_0 is the laser intensity. κ is the thermal conductivity of the embedded matrix.

$$Q_{MNP} = I_0 \sigma_{abs} \qquad . \tag{4.6}$$

$$\sigma_{abs}(\omega) = \frac{4\pi\omega\sqrt{\varepsilon_0}}{c} Im(a^3\gamma) \qquad . \tag{4.7}$$

σ_{abs} (equation 4.7) is the absorption cross section where ε_0 is the dielectric constant of the host material and γ is given by

$$\gamma = \frac{\varepsilon_m(\omega) - \varepsilon_0}{\varepsilon_m(\omega) + 2\varepsilon_0} \qquad . \tag{4.8}$$

$\varepsilon_m(\omega)$ is the dielectric function of the metal, which in our experiment is gold.

According to this model [28], the temperature changes 35K in gold spheres with 50nm radius and Δ=300nm separation for a light source with a wavelength of 514nm. Figure 6.7 shows variation of ΔT as function of laser intensity [28].

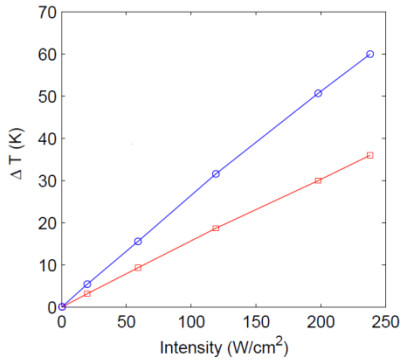

Figure 4.7 Temperature rise in the MNP sphere with 50nm radius and 300nm separation array, when the wavelength of the illuminating laser is 530nm (circles) or 514nm (square) [28].

By using other group's prediction [28] for emission spectra changes in similar QDs in presence of heat. We can plot the variation of peak emission single QDs, and FWHM at different temperatures are shown in Figure 4.8 [28]. These results suggest that even with a 60K temperature change for QD639, we should expect to see a 5nm red shift but from our experimental result we obtain a 9nm red shift. Also in our experimental result the FWHM increases 13nm for QD639 but Figure 4.8b suggests only a 3nm increase for a 60K temperature raise.

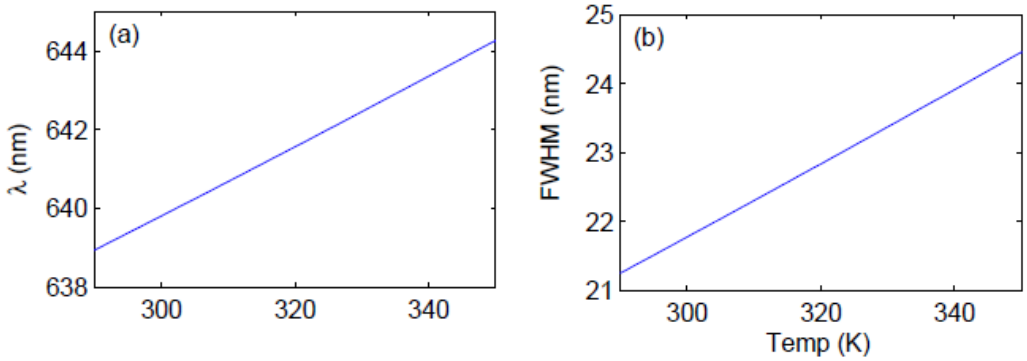

Figure 4.8 Variations in the (a) emission wavelength and (b) FWHM of the QD639 sample as a function of temperature [28] .

By comparing our experimental results with the calculated results from Figure 4.8 it can be seen that heat it is not the only factor that has an impact on the QDs' emission and other factors should contribute to the QDs' emission as well. Based on this calculation and our experimental result, the combined effects of the heat generated by the metallic nanoparticles and plasmons, lead to the collapse of the electrostatic barrier (Coulomb blockage) which is responsible to this abrupt change in QDs emission peak in the presence of MNPs [28].

4.4 PFE Enhancement of QDs

To investigate PFE and impact of plasmons, we study on QDs' emission in the presence and absence of MNPs as a function of time with different intensities. To do this we notice that the variation of QDs emission as a function of intensity in Figure 4.4 it has three regions. This figure suggests that in the intensity range of 0-50 W/cm^2 the peak emission of QDs increases linearly with the laser intensity due to the Photoinduced Fluorescence Enhancement (PFE). In Section 2.6 we explained how the PFE contributes to the enhancement of QDs emission. In the range of 50-70 W/cm^2, the peak emission shows a roll off on the emission curve. After 70 W/cm^2 the peak emission decreases significantly which suggests that the non radiative decay contributes more and the QY of QDs decreases. We study QDs emission as a function of time in all three ranges; increase, roll off, decrease; in the presence and absence of MNPs.

Figure 4.9-b shows the QDs' peak emission as a function of time in the absence of MNPs. Our experimental results in the absence of MNPs suggest that with a low laser

intensity 4 W/cm^2, QDs' peak emission in the first 10 minutes of irradiation, increases slowly. After the first 10 minutes the rate of increase in emission, decreases and stay constant. The increase in QDs' peak emission is due to the PFE. In PFE many processes such as heat, Oxidation, Surface passivation and Coulomb blockage are contributing factors.

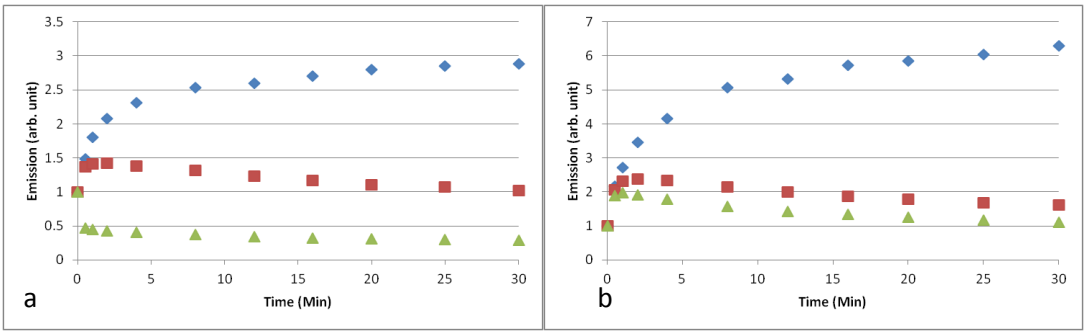

Figure 4.9 Variation of peak emission of QD639 as a function of time in the presence of MNPs (a) and in the absence of MNPs (b) for a laser intensity of 4 $\boldsymbol{W/cm^2}$ (rhombus), 60 $\boldsymbol{W/Cm^2}$ (square) and 160 $\boldsymbol{W/Cm^2}$(triangle) .

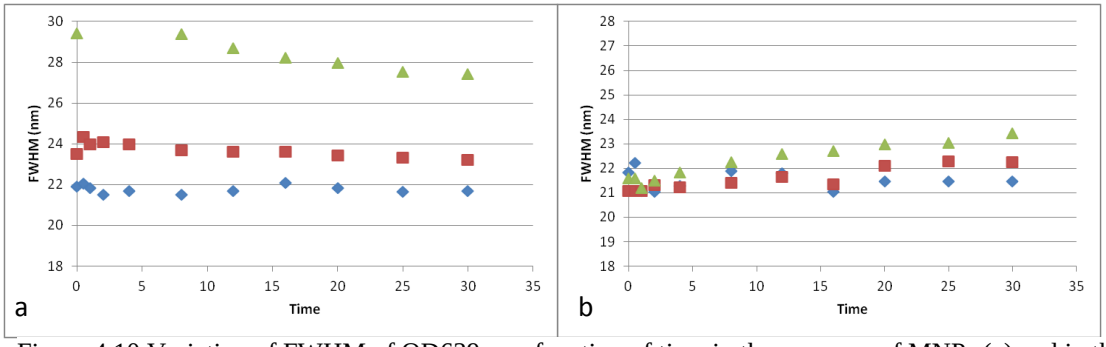

Figure 4.10 Variation of FWHM of QD639 as a function of time in the presence of MNPs (a) and in the absence of MNPs (b) for a laser intensity 4 W/cm^2 (rhombus), 60 W/cm^2 (square) and 160 W/cm^2(triangle).

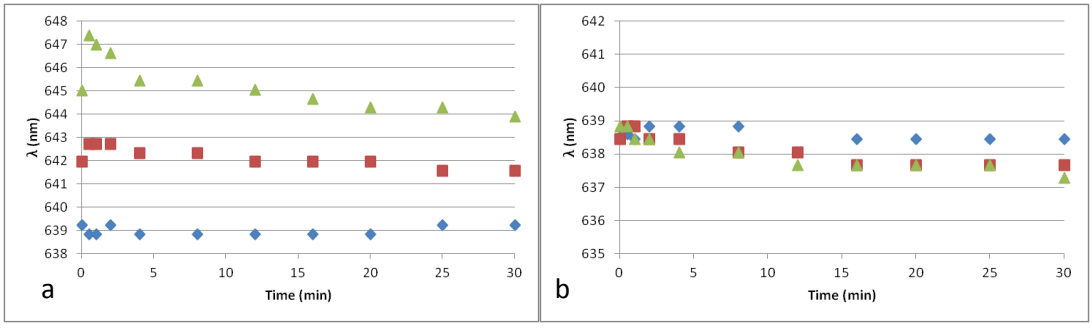

Figure 4.11 Variation of the emission wavelength of QD639 as a function of time in the presence of MNPs (a) and in the absence of MNPs (b) for a laser intensity 4 $\boldsymbol{W/cm^2}$ (rhombus), 60 $\boldsymbol{W/cm^2}$ (square) and 160 $\boldsymbol{W/cm^2}$(triangle).

The FWHM and the emission wavelength variations as a function of time in the presence and absence of MNPs are shown in Figures 4.10 and 4.11. Based on these figures in absence of MNPs, no broadening, blue shift or red shift is observed in QDs' emission at 4 W/cm^2 laser intensity. This indicates that heat and photo oxidation do not contribute to the PFE therefore it can be concluded that the enhancement of QDs' peak emission is due to Coulomb blockage. As laser intensity increases to 60 W/cm^2 (Figure 4.9-b,square), QDs' peak emission increases more rapidly but only in the first couple of minutes of irradiation and after that for a very short time a rolling off is seen and the peak emission starts to decrease. Figures 4.10b and 4.11b show that at this laser intensity, the FWHM starts to broaden and a small blue shift can be observed during the illumination, which indicates photo oxidation and heat, are starting to contribute in the PFE process.

One of the interesting aspects of our experimental result is when the QDs are illuminated with higher laser intensity. In this case the QDs' emission is significantly suppressed during the illumination period. We suggest that in high laser intensity more QDs are ionized in closed packed formation, and more photo-ionized QDs can lead to the collapse of electrostatic barriers, leading to significant nonradiative decay [28].

In addition, based on our experimental result in Figures 4.10b and 4.11b, an increase in laser intensity leads to an increase in blue shift and broadening in absence of MNPs which indicates that photo oxidation contributes more when laser intensity increases. In the presence of MNPs all of these processes happen faster and clearer due to the plasmonic FRET enhancement. PFE in QDs emission in presence of MNPs at the low intensity 4 W/cm^2 as it shown in Figure 4.9a-rhombus is less than PFE of QDs in

absence of MNPs. This is due to the FRET between QDs and MNPs that make coulomb blockages process less efficient during the time.

Also in high laser intensity, as we shown in Figure 4.9a-triangle QDs emission peak intensity drop from point 1 in initial time to point .5 after 30 seconds. This is due to QDs non-radiative decay through FRET between QDs and MNPs enhanced significantly and in overall QDs emission drops significantly. These phenomena indicate the collapse of the electrostatics barrier in vicinity MNPs [28].

CHAPTER 5

CONCLUSIONS

In this work, gold MNPs were fabricated via Annealing-Evaporation and EBL techniques. We optimized these techniques such that they led to plasmonic resonances that could cause significant enhancement of emission QDs with 639 nm wavelength. We studied emission of such QDs in presence and absence of MNPs as a function of time and laser intensity. Our experimental results showed in the vicinity of larger MNPs the emission of such QDs was enhanced more significantly than those QDs in the presence of smaller MNPs. This was consistent with our numerical results that suggested larger MNPs had larger scattering coefficients around the emission wavelength of the QDs than smaller MNPs.

In this research we studied, for the first time, how MNPs can influence photo-induced fluorescence enhancement (PFE) of QD solids. Our results showed that plasmonic near fields of MNPs could lead to abrupt activation of photoionization in such solids. This suggests that the coulomb blockage is not efficient in such solids when they in the vicinity of MNPs. We attributed this to the fact that near field of MNPs and FRET from QDs to MNPs could reduce the efficiency of such a blockage.

REFERENCES

[1] A.R. Santos, A.S. Miguel, L. Tomaz, R. Malhó, C. Maycock, M.C. Vaz Patto, P. Fevereiro, and A. Oliva, "The impact of CdSe/ZnS Quantum dots in cells of Medicago sativa in suspension culture," *Journal of Nanobiotechnology*, vol. 8, Jan. 2010, p. 24.

[2] M. A. Walling, J. A. Novak, and J.R.E. Shepard, "Quantum dots for live cell and in vivo imaging," *International Journal Of Molecular Sciences*, vol. 10, Mar. 2009, pp. 441-91.

[3] G.Rao and A. Bluma,"Optical sensor system in biotechnology," Springer, 2009.

[4] E. Hutter and J.H. Fendler, "Exploitation of localized surface plasmon resonance," *Advanced Materials*, vol. 16, Oct. 2004, pp. 1685-1706.

[5] J.D. Jackson, "Classical Electrodynamics," Wiley 1999.

[6] http://nanohub.org/resources/1748

[7] C. Kittel, "Introduction to Solid State Physics," Wiley, 2005.

[8] K. A. Willets and R.P. Van Duyne, "Localized surface plasmon resonance spectroscopy and sensing.," *Annual Review Of Physical Chemistry*, vol. 58, Jan. 2007, pp. 267-97.

[9] K. Matsubara, S. Kawata, and S. Minami, "Optical chemical sensor based on surface plasmon measurement" *Applied Optics*, vol. 27, 1988, pp. 1160-1163.

[10] S. Shen, T. Liu, and J. Guo, "Optical phase-shift detection of surface plasmon resonance" *Applied Optics*, vol. 37, Apr. 1998, pp. 1747-51.

[11] S. Roh, T. Chung, and B. Lee, "Overview of the characteristics of Micro-and Nano-structured surface plasmon resonance sensor," *Sensor*, 2011, 11(2), pp1565-1588

[12] S. Patskovsky, A.V. Kabashin, M. Meunier, and J.H.T. Luong, "Properties and sensing characteristics of surface-plasmon resonance in infrared light," *Journal of the Optical Society of America. A, Optics, Image Science, And Vision*, vol. 20, Aug. 2003, pp. 1644-50.

[13] S.M. Sadeghi, R.G. West, and A. Nejat, "Photo-induced suppression of plasmonic emission enhancement of CdSe/ZnS quantum dots," *Nanotechnology*, vol. 22, Oct. 2011, p. 405202.

[14] D. Sarid and W. Challener, "Moder Introduction to Surface Plamsons: Theory, Mathematcial Modeling and Applications," Cambridge University Press, 2010.

[15] V.I. Klimov, "Nanocrystal Quantum Dots, Second Edition," *Los Alamos Science*, Apr. 2010, pp. 214-220.

[16] C.B. Murray, C.R. Kagan, and M. G. Bawendi "Synthesis and characterization of monodisperse nanocrystals and close-packed nanocrystal assemblies*" Ann. Rev. Mater. Sci.* 2000. 30 pp. 540-610.

[17] S.M. Sadeghi, "Tunable nanoswitches based on nanoparticle meta-molecules," *Nanotechnology*, vol. 21, Sep. 2010, p. 355501.

[18] H. Pan, R. Cui, and J.-J. Zhu, "CdTe quantum dots as probes for near-infrared fluorescence biosensing using biocatalytic growth of Au nanoparticles," *The Journal Of Physical Chemistry. B*, vol. 112, Dec. 2008, pp. 16895-901.

[19] http://www.ecse.rpi.edu/~schubert/Course-ECSE 6968%20Quantum%20mechanics/Ch12%20Density%20of%20states.pdf

[20] P. G. Anikeeva," Physical Properties and Design of Light-Emitting Devices Based on Organic Materials and Nanoparticles: A Thesis," Massachusetts Institute of Technology 2009.

[21] C. Higgins, M. Lunz, A. L. Bradley, V. A. Gerard, S. Byrne, Y.K. Gun'ko, V. Lesnyak, and N. Gaponik, "Energy transfer in colloidal CdTe quantum dot nanoclusters," *Optics Express*, vol. 18, Nov. 2010, pp. 24486-24494.

[22] C. Carrillo-Carrión, S. Cárdenas, B.M. Simonet, and M. Valcárcel, "Quantum dots luminescence enhancement due to illumination with UV/Vis light," *Chemical communications (Cambridge, England)*, Sep. 2009, pp. 5214-26.

[23] S. Maenosono, "Modeling photoinduced fluorescence enhancement in semiconductor nanocrystal arrays," *Chemical Physics Letters*, vol. 376, Jul. 2003, pp. 666-670.

[24] S. Link and M. A. El-Sayed, "Shape and size dependence of radiative, non-radiative and photothermal properties of gold nanocrystals," *International Reviews in Physical Chemistry*, vol. 19, Jul. 2000, pp. 409-453.

[25] C. F. Bohren and D. R. Huffman," Absorption and Scattreing of Light by Smaill Particles,"Appendix A, Wiley, 1983.

[26] C.J. Jia and F. Schuth, " Colloidal metal nanoparticles as component of designed catalyst," *Phys. Chem. Chem. Phys*, 2011,13,pp. 2457-2487.

[27] http://www.nn-labs.com/

[28] S.M. Sadeghi and A. Nejat, “Abrupt Plasmonic Activation of Photoionization Rates in Quantum Dot Solids,” *J. Phys. Chem. C*, 2011, 115 (44), pp 21584–21591.

[29] A.O. Govorov, G.W. Bryant, W. Zhang, T. Skeini, J. Lee, N. A. Kotov, J.M. Slocik, and R.R. Naik, “Exciton−plasmon interaction and hybrid excitons in semiconductor−metal nanoparticle assemblies,” *Nano Letters*, vol. 6, May. 2006, pp. 984-994.

[30] A.O. Govorov, W. Zhang, T. Skeini, H. Richardson, J. Lee, N. A. Kotov, *Nanoscale Res. Lett*. 2006, 1, 84.